SANDIA REPORT
SAND2012-0103
Unlimited Release
Printed January 2012

Real-time Studies of Battery Electrochemical Reactions Inside a Transmission Electron Microscope

John P. Sullivan, Jian Yu Huang, Kevin Leung, Mike J. Shaw, Hong You Fan, Arunkumar Subramanian, Xiao Hua Liu, Yang Liu, and Nicholas S. Hudak

Prepared by
Sandia National Laboratories
Albuquerque, New Mexico 87185 and Livermore, California 94550

Sandia National Laboratories is a multi-program laboratory managed and operated by Sandia Corporation, a wholly owned subsidiary of Lockheed Martin Corporation, for the U.S. Department of Energy's National Nuclear Security Administration under contract DE-AC04-94AL85000.

Issued by Sandia National Laboratories, operated for the United States Department of Energy by Sandia Corporation.

Available to DOE and DOE contractors from
U.S. Department of Energy
Office of Scientific and Technical Information
P.O. Box 62
Oak Ridge, TN 37831

Telephone: (865) 576-8401
Facsimile: (865) 576-5728
E-Mail: reports@adonis.osti.gov
Online ordering: http://www.osti.gov/bridge

Available to the public from
U.S. Department of Commerce
National Technical Information Service
5285 Port Royal Rd.
Springfield, VA 22161

Telephone: (800) 553-6847
Facsimile: (703) 605-6900
E-Mail: orders@ntis.fedworld.gov
Online order: http://www.ntis.gov/help/ordermethods.asp?loc=7-4-0#online

SAND2012-0103
Unlimited Release
Printed January 2012

Real-time Studies of Battery Electrochemical Reactions Inside a Transmission Electron Microscope

J. P. Sullivan, J. Y. Huang, A. Subramanian, X. H. Liu, and Y. Liu
CINT Science Department

K. Leung
Surface and Interface Sciences Department

M. J. Shaw
MEMS Technologies Department

H. Y. Fan
Ceramic Processing and Inorganic Department

N. S Hudak
Advanced Power Sources R & D Department

Sandia National Laboratories
P.O. Box 5800
Albuquerque, NM 87185

Abstract

We report the development of new experimental capabilities and *ab initio* modeling for real-time studies of Li-ion battery electrochemical reactions. We developed three capabilities for *in-situ* transmission electron microscopy (TEM) studies: a capability that uses a nanomanipulator inside the TEM to assemble electrochemical cells with ionic liquid or solid state electrolytes, a capability that uses on-chip assembly of battery components on to TEM-compatible multi-electrode arrays, and a capability that uses a TEM-compatible sealed electrochemical cell that we developed for performing *in-situ* TEM using volatile battery electrolytes. These capabilities were used to understand lithiation mechanisms in nanoscale battery materials, including SnO_2, Si, Ge, Al, ZnO, and MnO_2. The modeling approaches used *ab initio* molecular dynamics to understand early stages of ethylene carbonate reduction on lithiated-graphite and lithium surfaces and constrained density functional theory to understand ethylene carbonate reduction on passivated electrode surfaces.

ACKNOWLEDGMENTS

This work was supported by a Laboratory Directed Research and Development (LDRD) project at Sandia National Laboratories and partly by the Science of Precision Multifunctional Nanostructures for Electrical Energy Storage (NEES), an Energy Frontier Research Center funded by the U.S. Department of Energy, Office of Science, Office of Basic Energy Sciences under Award Number DESC0001160. In addition, this work was performed, in part, at the Sandia-Los Alamos Center for Integrated Nanotechnologies (CINT), a U.S. Department of Energy, Office of Basic Energy Sciences user facility. We would like to thank S. Hearne, K. Zavadil, G. Nagasubramanian, D. Ingersoll, J. Nogan, D. Huber, S. Limmer, W. Yelton, S. Mao, J. Li, T. Zhu, S. Zhang, J. Lou, Y. Qi, J. Cumings, C. Wang, G. Gulley, P. Balbuena, S. George, A. Dillon, C. Wang, T. Picraux, L. Zhong, W. Xu, L. Zhang, L. Qi, A. Kushima, G. Wang, Z. Ye, S. Huang, L. Gui, Y. Zhan, K. Karki, W. Liang, J.-H. Cho, E. Epstein, X. Qian, Y. Jung, A. Cavanagh, S. Lee, G. Zhu, and Z. Wang for assistance with ideas, materials, techniques, experiments, and equipment. Sandia National Laboratories is a multi-program laboratory managed and operated by Sandia Corporation, a wholly owned subsidiary of Lockheed Martin company, for the U.S. Department of Energy's National Nuclear Security Administration under contract DE-AC04-94AL85000.

CONTENTS

FIGURES

NOMENCLATURE

AIMD	*ab initio* molecular dynamics
DEP	dielectrophoresis
DFT	density functional theory
DOE	Department of Energy
EC	ethylene carbonate
LIB	Li-ion battery
MD	molecular dynamics
MEMS	microelectromechanical systems
MWCNT	multi-wall carbon nanotubes
NW	nanowire
SEI	solid electrolyte interphase
SNL	Sandia National Laboratories
TEM	transmission electron microscope/microscopy

THIS PAGE

INTENTIONALLY BLANK

1. INTRODUCTION

The purpose of this project was to develop new capabilities to measure and understand electrochemical mechanisms in electrochemical energy storage systems (batteries). This project was motivated by the global need to improve the energy density, power density, and reliability of energy storage systems in order to meet goals for the expansion of green energy technologies. Given their high gravimetric energy density and good reversibility, Li-ion cells have received some of the greatest interest, but there are critical scientific challenges related to the capacity and lifetime of the cathodes and anodes, degradation after cycling, and high temperature stability. The fundamental study of electrochemical phenomena in this system has been hampered by the great lack of experimental and theoretical techniques that can identify structural changes in battery materials with atomic to nano-scale resolution during actual battery operation. To meet these needs, we developed experimental tools to enable the investigation of Li-ion battery electrochemical processes in real time inside a transmission electron microscope (TEM), using both (1) a novel sealed silicon micromachined fluidic platform and (2) a simple open platform using a vacuum-stable ionic liquid (IL) electrolyte. We also used *ab initio* molecular dynamics (MD) and constrained density functional theory (DFT) to model the formation of solid electrolyte interphase (SEI) reaction products on unpassivated lithiated carbon and lithium metal anodes and on passivated lithiated carbon anodes.

1.1. Background

Currently, Li-ion batteries offer great promise for achieving near-term goals for high specific energy storage – expressed as Wh/kg – in a rechargeable cell. For example, the near-term goal for batteries for high-volume electric vehicle production, as defined by the U.S. Advanced Battery Consortium, is 150 Wh/kg,[1] and Li-ion cells with specific energies up to 150 Wh/kg have been available commercially since the early 1990's.[2,3] In addition, there is substantial room for improvement in the charge capacity of Li-ion cells, particularly on the anode side where charge storage capacities could be improved by factors of two to three, resulting in as much as a 50% improvement in cell specific energy.[4] Despite the promise of this technology, there are still challenges with cell lifetime, particularly with the newer high-capacity anodes and cathodes. For example, alloy or conversion anodes, e.g. Si, Sn, Fe_2O_3, etc., which exhibit large volume changes during cycling, often show large capacity loss after the first cycle and shorter cycling lifetimes.[5] From a purely economic perspective, the requirement for long lifetime is at least as important as high specific energy. Any cost savings from doubling the specific energy of a battery module is lost if the module only lasts half as long as the required lifetime. Therefore, research on new Li-ion battery technologies must occur in concert with studies of fundamental mechanisms that control battery performance and reliability.

Although the degradation mechanisms in Li-ion cells are numerous and diverse, we will consider an arbitrary and, admittedly, over-simplified grouping into three regions of interest: reactions at the electrode/electrolyte interface, structural and mechanical changes in the electrodes, and chemical changes in the electrolyte. Intensive research activities are ongoing in all three areas; however, we will limit our discussion to the first two regions for the practical reason that the subject of this work is focused on solid-state materials.

Reactions at the electrode/electrolyte interface are ubiquitous for high voltage Li-ion cells, the most well-known being the formation of the solid-electrolyte interphase (SEI). The SEI is a reaction product of mixed composition commonly found on highly-negative anodes, e.g. Li metal or graphite-lithium intercalation compounds.[6] The SEI layer forms as a result of electrochemical reduction of the electrolyte and formation of insoluble reaction products. Growth typically becomes self-limited due to the low electronic conductivity of the mostly ionic reaction compounds. Equivalently, SEI reaction products may also form on high voltage cathodes, but the mechanisms are different, e.g. oxidation of the electrolyte or oxidation of reaction products dissolved at the anode and then precipitated at the cathode.[7,8] Key points to consider regarding the SEI layers are that: 1) the nature and composition of the SEI layer is electrolyte-dependent, 2) the SEI typically forms and grows during cell charging and discharging, and it may or may not reach a stable structure until after several cycles, 3) the presence of and the stability (as a function of time and temperature) of the SEI can play an important role in cell stability (acute failure) and cell long-term degradation. The study of the SEI layer requires the use of the common Li-ion electrolytes, e.g. ethylene carbonate-based solution, probes that have sufficient spatial resolution to detect the presence of a reaction product layer just a few nm thick, and the ability to monitor the changes in SEI layer with cycling and, perhaps, time and temperature. These requirements drive the development of the MEMS-based *in-situ* characterization platform that we describe below.

An additional type of degradation mechanism in battery electrodes is related to the mechanical and structural changes that occur as a result of electrochemical cycling. These degradation mechanisms are particularly acute for the newer high-capacity anodes and cathodes. For example, Li-alloy electrodes, such as the Sn-based or Si-based anodes, undergo large volume expansion up to a few hundred percent during initial reaction with Li.[5] Such large volume changes are difficult to accommodate in bulk or thin materials of high density, and this leads to a variety of mechanical failure modes, e.g. plasticity, cracking, spallation, and ultimately loss of electrical contact of the anode particle with the current collector. In addition fracture of the active material exposes new surfaces to the electrolyte. This leads to spontaneous additional SEI formation and a loss of capacity. In large part, one reason for the commercial success of the intercalation/insertion cell, graphite/$LiCoO_2$, may be attributed to the fact that these materials undergo only modest volume change during cycling compared to higher Li-content materials. However, the capacity of intercalation and insertion anode and cathode materials is ultimately limited, and this has driven the search for newer materials that alloy or form reaction compounds with Li. Hence we will see increasing mechanical degradation failure modes with increased utilization of new materials.

One solution to the large volume changes that occur in high capacity anode and cathode materials is the creation of nanoscale or nanostructured particles of the electroactive phase. Nanoscale objects, such as nanowires, often pack at lower density, providing void area that is then able to accommodate the large volume changes during cycling. This enables the electroactive phase to remain as a contiguous, though possibly highly-modified, structure during cycling. A good example of the use of nanoscale electroactive materials are silicon nanowire anodes that retain high capacity during several charge-discharge cycles, despite an initial volume change of 400%.[9] In contrast, bulk silicon loses more than 80% of its capacity in less than 10 cycles, primarily due to pulverization.[10]

The mechanical "compliance" of nanoscale materials may lead to their increasing utilization in Li-ion batteries. Furthermore, there are other reasons for interest in nanoscale electroactive phases, such as the potential to reduce cell impedance and increase power capabilities. One of the best examples is nanoscale $LiFePO_4$ particles as cathodes that demonstrate both acceptably low electrical impedance and high rate capability.[11]

Regardless of the reason for the use of nanoscale materials in batteries, their use introduces challenges for structural and electrochemical characterization. Their small physical dimension (nm to 10's of nm) and size-dependent properties require utilization of probes with nm or better spatial resolution. This is particularly important if we wish to examine mechanisms of charge storage or degradation at the single particle level, as opposed to averaging over an ensemble of particles. While traditional electrochemical tests, such as charge-discharge cycling, cyclic voltammetry, or electrochemical impedance spectroscopy, are *de rigeuer* for characterizing battery performance, these tests do not provide insight into mechanisms at the atomic to nano-scale (scanning electrochemical microscopy, excepted). To provide this atomic to nanometer resolution, we have developed new platforms for enabling electrochemical characterization while imaging inside a high resolution transmission electron microscope (TEM). The use of TEM for studying battery materials is, of course, widespread.[12] The challenge is to create platforms and techniques that enable TEM imaging while simultaneously performing electrochemical testing, i.e. *in-situ* TEM characterization. The development of new characterization tools is an area of need in battery research. For example, in the comprehensive review of Li-ion batteries by Tarascon et al., he specifically cites this need in his summary statements, "The principal challenge for Li-based rechargeable batteries, or indeed for any battery, lies in gaining better understanding and control of the electrode-electrolyte interface in the hope of designing new solid-solid or solid-liquid interfaces. … Efforts aimed at developing new characterization tools must be vigorously pursued …".[4] It is hoped that by developing new characterization approaches with atomic to nano-scale spatial resolution, we will be able to generate new insight into the mechanisms of storage and degradation in Li-ion batteries.

1.2. Summary of Accomplishments

In this report, we describe accomplishments in several areas related to understanding Li-ion battery electrochemical mechanisms at the atomic to nano-scale. We first describe our recent accomplishments in understanding chemical pathways that lead to the formation of the SEI layer on anode materials. The first modeling results used *ab initio* MD to identify the chemical reactions when ethylene carbonate molecules are reduced at the surface of oxygen-terminated lithiated graphite (LiC_6) or lithium metal. This work revealed a new, unrecognized reaction mechanism that leads to CO formation during initial SEI formation. Subsequent modeling results examined later stages of SEI formation – the formation of SEI on passivated anode surfaces. These simulations used LiC_6 surfaces that were passivated with $LiAlO_2$ (an artificial SEI), and a combination of constrained DFT and Marcus theory identified the dominant reaction product as well as an estimate for the reaction rate (which was found to be ~9 orders of magnitude lower than the EC decomposition rate on the unpassivated surface).

Second, we describe the development of an *in-situ* TEM electrochemistry capability based on the use of a nanomanipulator to assemble an electrochemical cell inside a TEM that consists of

battery materials [e.g. tin oxide, silicon, zinc oxide, and aluminum anode nanoparticles and nanowires (NWs)], a Li-containing counter electrode (Li or Li cobalt oxide), and an ionic liquid electrolyte or a solid-state electrolyte (Li_2O). After cell assembly, we identified several remarkable electrochemical mechanisms associated with anode lithiation and delithiation. We identified the strain accommodation mechanisms in conversion anodes, identifying new behavior such as a dislocation-induced amorphization of the crystalline anode phase. We also observed diffusion anisotropy in silicon anodes and identified the role of electrical conductivity in influencing the silicon lithiation rate. We identified failure mechanisms associated with cracking in silicon and the quite different mechanism of vacancy coalescence and void formation in the related material, germanium. In addition, we observed that thin aluminum oxide layers that are used to create an artificial solid-electrolyte-interphase (SEI) layer react with Li and act as an effective solid electrolyte, providing a conduit for lithiation of the underlying material.

Third, we describe the development of two additional *in-situ* TEM electrochemistry platforms: (1) a multi-electrode, chip-based, TEM-compatible platform for assembling battery nanoparticles using dielectrophoresis (DEP) on to electrodes for subsequent electrochemical, electrical, and structural characterization and (2) a new MEMS-based liquid cell platform for *in-situ* TEM studies that permits electrochemistry inside a TEM using conventional (volatile) electrolytes. The first of these platforms was used to understand the structural changes that occur during the initial lithiation of a β-MnO_2 cathode NW. The second platform was successfully fabricated and tested using TEM imaging of a liquid cell that was filled with an ethylene carbonate-based battery electrolyte.

1.3. Significance

The work in this project has led to the development of a new capability in the area of electrochemical energy storage, a capability that enables one to view and understand electrochemical reactions in real-time with atomic scale resolution. In addition we developed sophisticated MEMS-based electrochemical cells that permit an even greater variety of electrochemical reactions to be observed inside a TEM, specifically electrochemical reactions involving common electrolytes, such as water or ethylene carbonate mixtures, which normally cannot be used in the vacuum environment of the TEM. Equally importantly, we developed sophisticated modeling techniques based on *ab initio* MD (AIMD) that permit the identification and prediction of reaction products that form at electrode-electrolyte interfaces. Using these capabilities, we have identified important electrochemical reaction mechanisms in Li-ion battery materials as they lithiate and delithiate and interfacial reactions between ethylene carbonate electrolytes and Li-ion battery anode phases. This work leads to important suggestions on how to improve the performance and lifetime of Li-ion batteries. This is critical for meeting Dept. of Energy (DOE) goals in advancing the use of clean energy technologies. At Sandia, this project has led to the creation of a strategic area of excellence in *in-situ* characterization for batteries. This work is an important part of Sandia's Energy Storage Roadmap and has led to new funded initiatives that aim to use the capabilities developed in this project for understanding the mechanisms of battery degradation.

2. *AB INITIO* MODELING OF SEI FORMATION MECHANISMS

In this section, we describe our results using *ab initio* modeling techniques to examine the chemical reaction pathways during the initial and later stages of SEI formation from ethylene carbonate solvents in contact with Li-ion battery anode phases. This work has been published and is available in print. Therefore, we only highlight the work here and refer the reader to the referenced journal publications for further details.

2.1. *Ab Initio* MD of EC/Graphite Interfaces

We identified the decomposition pathway for liquid ethylene carbonate (EC) molecules on the surface of oxygen-terminated lithiated graphite (LiC_6) using *ab initio* MD (AIMD).[13] We found that the graphite edge site chemical termination (the chemical species on the edges of the graphite basal planes) play an important role in influencing the reaction pathway, with the oxygen-terminated carbon edges supporting the rapid reduction of EC to produce a primary decomposition pathway that liberates carbon monoxide (CO), see Figure 1. These findings illustrated the success that can be achieved using AIMD techniques to model the initial stages of SEI formation (the reaction rates are sufficiently fast to be observed in simulation times of several picoseconds), and these AIMD results identified an important reaction pathway, two electron reduction leading to CO formation, that has been observed experimentally but not predicted prior to this study.

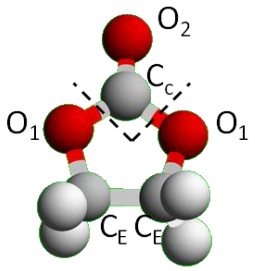

Figure 1. AIMD indicates that cleavage of the C_c-O_1 bonds is the primary reduction mechanism, liberating CO.

2.2. *Ab Initio* MD of EC/Lithium Interfaces

We used hybrid density functional theory (DFT) functional to examine electron localization and bond breaking for excess electrons on EC both in the pure liquid state and at lithium metal interfaces.[14] We found that in the liquid state, electron attachment on to an EC^- anion with a broken C_E-O_1 bond leads to the breaking of additional C_E-O_1 bond and the formation of CO_3^{2-} and C_2H_4 fragments (see Fig. 1 for labeling) while EC reduction at a Li metal surface still favors EC decomposition to form CO similar to what was observed for the LiC_6 interface, see Figure 2.

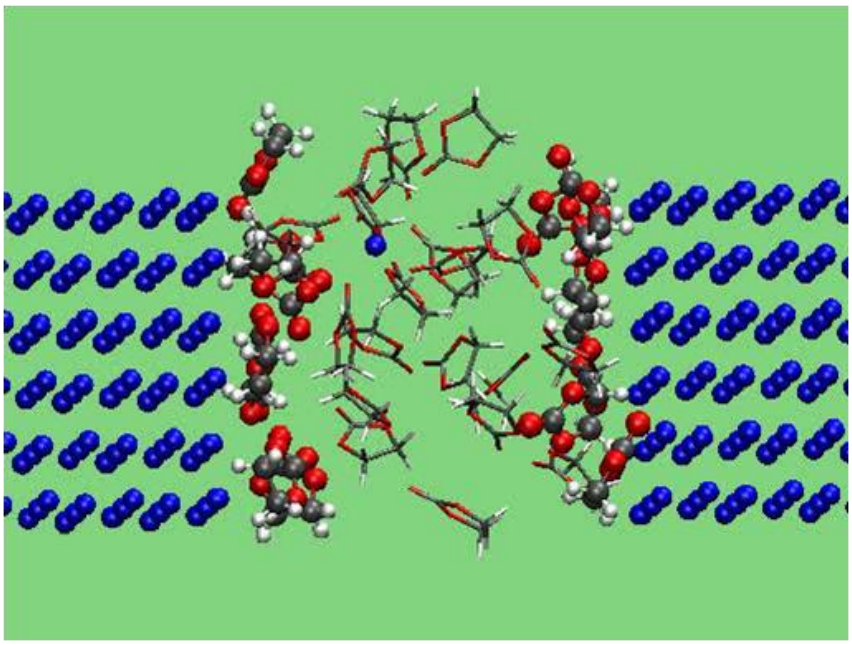

Figure 2. AIMD simulation of EC at Li metal surfaces. EC molecules that have reacted are depicted using large ball-and-stick structures (in contrast to unreacted EC shown as stick structures).

2.3. Modeling of SEI Formation on Passivated Anodes

Our modeling results show that EC molecules react promptly on unpassivated anode surfaces (LiC_6 or Li^0) resulting in a dominant reduction pathway that produces CO. In real Li-ion battery systems, this prompt reduction of EC leads to the accumulation of reaction product on the anode surface that is known as the SEI. This SEI layer acts as a solid electrolyte, permitting the transport of Li+ ions while hindering electron transport. Thus the SEI acts as a passivating layer that limits further EC reduction. In order to understand EC reduction in the presence of a passivated anode surface, we performed *ab initio* calculations of EC reduction at an LiC_6 surface that was coated with an artificial SEI, a thin layer of $LiAlO_2$.[15] These calculations were compared to experimental efforts from the Dillon and George group (the use of atomic-layer deposited Al_2O_3 as an artificial SEI) and Zavadil (electrochemical measurements of SEI formation on passivated surfaces). Using constrained DFT, we found that ~ 1 nm of $LiAlO_2$ is sufficient to reduce the EC reduction rate by 9 orders of magnitude compared to the unpassivated surfaces, and we find that the dominant reduction product shifts from CO (observed on the unpassivated surfaces) to CO_3^{2-}, see Figure 3.

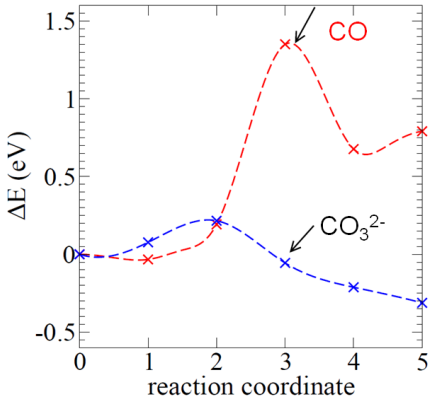

Figure 3. The reaction pathway to produce CO_3^{2-} is favored over CO production for EC reduction on passivated (e.g. SEI-covered) anodes. This plot was generated assuming a coverage of 1 nm of $LiAlO_2$ on LiC_6.

3. *IN-SITU* TEM STUDIES

In this section, we describe our results in developing and using *in-situ* TEM techniques to explore the electrochemistry of Li-ion battery materials. This work has been published and is available in print. Therefore, we only highlight the work here and refer the reader to the referenced journal publications for further details.

One of the cornerstones of the work we describe here is the development of an experimental capability to measure electrochemical reactions inside the TEM. This was achieved through the use of a TEM nanomanipulator to assemble an electrochemical cell consisting of a nanoscale working electrode (typically a nanowire Li-ion battery anode material), a counter electrode that contains lithium (typically a particle of $LiCoO_2$ or Li metal), and an electrolyte, either an ionic liquid based electrolyte containing a dissolved salt of lithium, such as Li-TFSI or a solid electrolyte, such as a very thin layer of Li_2O. Figure 4 shows a schematic of this *in-situ* TEM cell as well as images depicting the actual preparation of an *in-situ* TEM Li-ion battery cell. This is the cell configuration that was used for the results described in the followed sub-sections.

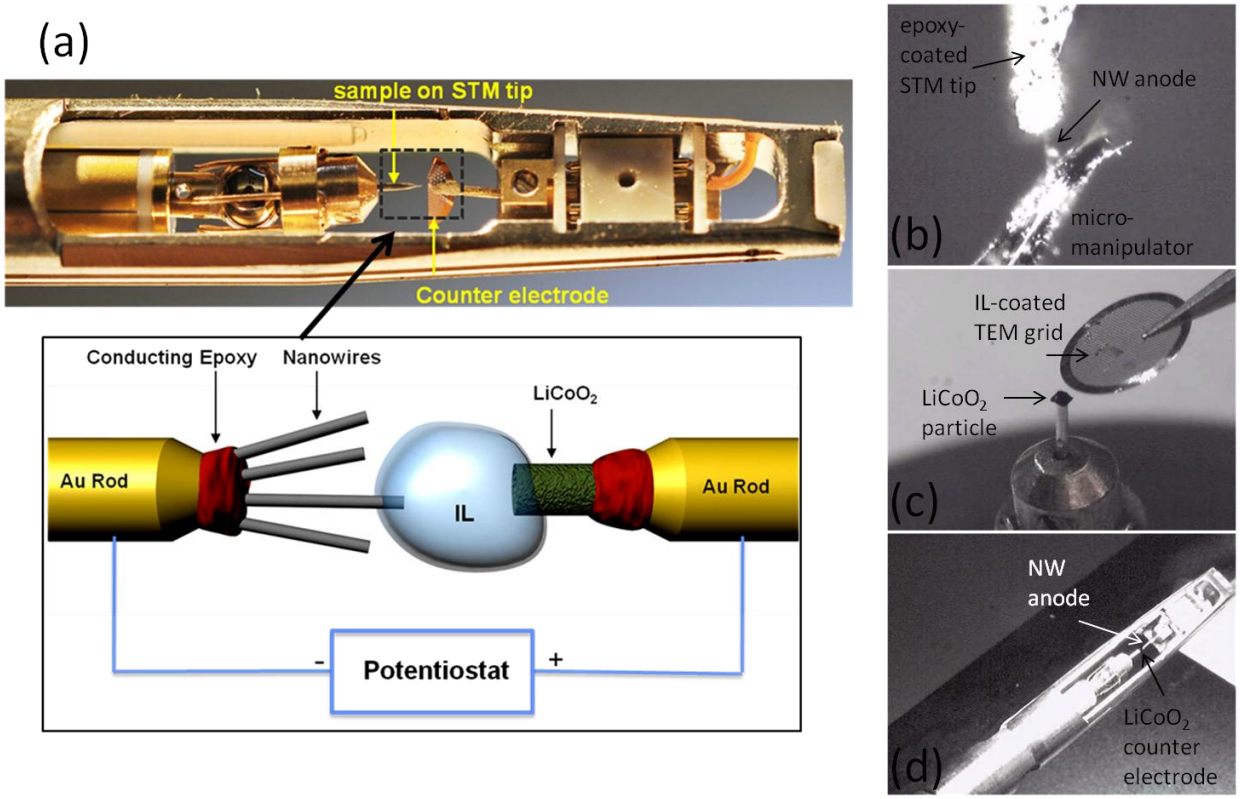

Figure 4. (a) Schematic of the *in-situ* TEM cell using ionic liquids (IL) as an electrolyte. The cell is assembled using an *in-situ* TEM nanomanipulator –a scanning tunneling microscope (STM) tip on an *in-situ* TEM STM holder. To assemble the cell, (b) a micro-manipulator is used to place a single NW anode or a bundle of anode NWs on to an epoxy-coated STM tip. (c) The counter electrode is assembled by placing a droplet of IL on to a $LiCoO_2$ particle. (d) The IL-coated $LiCoO_2$ particle and the NW on the STM tip are assembled on to the TEM holder.

3.1. *In-situ* TEM of SnO_2 Lithiation

We used the in-situ TEM cell with an ionic liquid electrolyte to identify the structural changes that occur during the lithiation of a SnO_2 Li-ion battery (LIB) anode.[16] Starting with a single crystal SnO_2 nanowire anode, we observed that lithiation induces a transformation of the SnO_2 into amorphous Li_2O and nanocrystals of Li_xSn alloy. There is a large volume change for this conversion reaction, about 240% expansion, that is primarily manifested as a lengthening of the NW, see Figure 5. In order to accommodate the large radial expansion, about 45%, a high density of dislocations are nucleated at the c-SnO_2/a-Li_2O interface. These dislocations eventual terminate at the c-SnO_2 surface about one to two NW diameters from the interface. The dislocation density is high enough to cause amorphization of the SnO_2 near the reaction interface. Delithiation of the anode leads to loss of Li from the Li_xSn nanocrystals, but no reduction of the a-Li_2O. The volume change following delithiation is small.

In a subsequent study, we examined the lithiation process of the SnO_2 NW in the zone that was fully immersed in the IL electrolyte.[17] We observed the formation of multiple stripes of lithiation that progress across the NW along the (020) planes. The stripes increase in density with further lithiation, eventually merging and resulting in the a-Li_2O phase and morphology that is observed in the SnO_2 NW outside the immersion zone. Furthermore, the application of coatings on to the SnO_2 NWs in the form of carbon, aluminum, or copper greatly alter the morphology and defect structure following lithiation.[18] These coatings enhance the electrical conductivity of the NWs, increasing the lithiation rate by about a factor of 10 and suppressing both the radial expansion and the generation of dislocations at the SnO_2/Li_2O interface. These results suggest that composite LIB anodes can be engineered to have remarkably different performance than the monolithic structures.

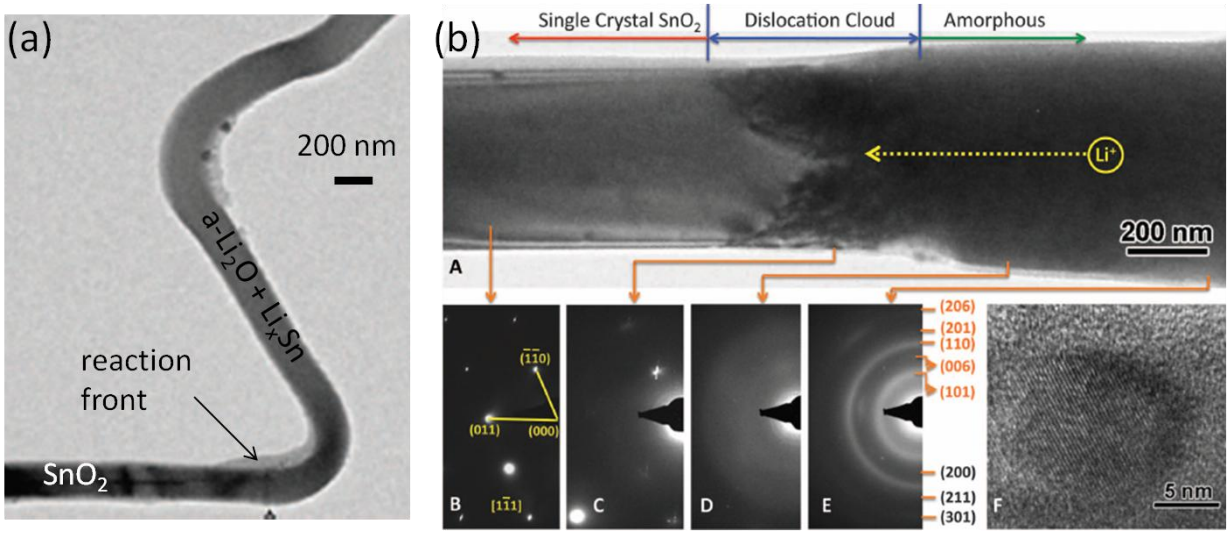

Figure 5. (a) Morphology of the SnO_2 anode following lithiation and the formation of a-Li_2O and nanocrystals of Li_xSn. (b) High magnification image of the interface region (from ref. [16]).

3 .2. *In-situ* TEM of Si Lithiation

Silicon is of great interest as an anode material for LIBs due to its high theoretical capacity, ~ 3579 mAh/g for the $Li_{15}Si_4$ phase. We used *in-situ* TEM to observe the lithiation mechanisms, defect structure, and reaction rates for Si NW anodes. For single crystal Si NW anodes, we observed that the lithiation rate is highly anisotropic, which leads to distinct morphological

changes; specifically, the lithiation rate normal to the (111) planes is slow.[19] For Si NWs with an axial orientation along [112], lithiation leads to the formation of Li_xSi with a distinct bi-lobed or dumbbell-shaped cross-section. Due to this bilobed structure, cracks can nucleate along the NW axis leading to bifurcation of the wire.

In an additional study, we examined the effect of surface coating and electronic doping to enhance the lithiation rate of Si NWs.[20] We found that the combination of electronic doping and surface coating with carbon could lead to an order of magnitude increase in the lithiation rate of Si NWs. The lithiation progresses by a core-shell process where the large volume expansion required to form Li_xSi (~ 300 %) is accommodated by the progression of a lithiation front from the surface inward to the core and a large radial expansion, up to 260% for some crystallographic directions, see Figure 6. At high lithiation rates, the amorphous Li_xSi alloys crystallizes into $Li_{15}Si_4$, the highest Li-content phase we observed.

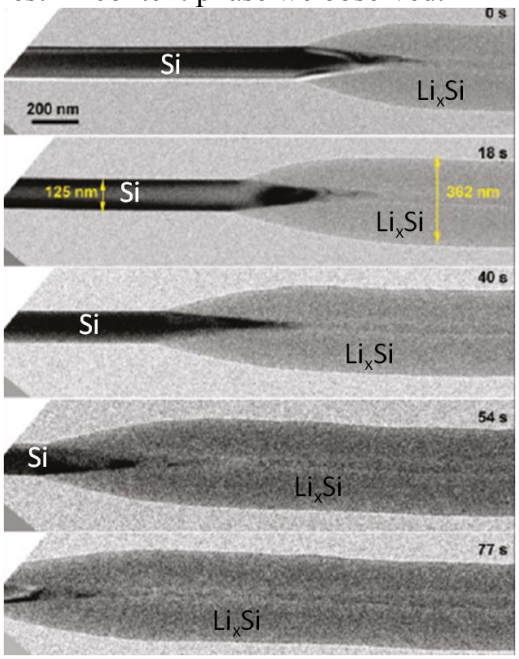

Figure 6. The morphology of Si NWs following lithiation. The lithiation front progresses from the surface towards to the center, accompanied by a large radial expansion associated with the formation of Li_xSi (from ref. [20]).

3.3. *In-situ* TEM of Ge Lithiation

While Si anodes for LIBs demonstrate very high gravimetric capacity, the cycle life is often found to be limited due to mechanical effects, such as cracking and pulverization of the Si. In contrast, Ge possesses a lower gravimetric capacity, 1384 mAh/g, but appears to offer higher cycle life. We have performed in-situ TEM studies of the lithiation mechanisms and cycling performance of Ge NWs.[21] We found that Ge NWs exhibit very different lithiation and delithiation mechanisms compared to Si. Specifically, the single crystal Ge NWs initially transform to amorphous Li_xGe and then crystalline $Li_{15}Ge_4$ with lithiation. Upon delithiation, the NWs form an internal nanoporous network consisting of nanoscale voids that likely form as a result of a de-alloying process, see Figure 7. This nanoporous network is preserved during subsequent lithiation-delithiation cycling, leading to a robust morphology that is resistant to mechanical degradation. This suggests that Ge LIB anodes may exhibit superior cycling lifetime compared to Si anodes.

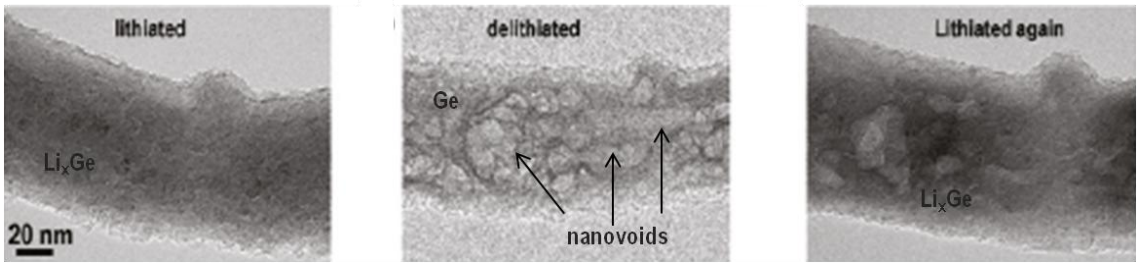

Figure 7. Lithiated Ge NWs exhibit a nanoporous morphology following delithiation which is preserved in subsequent cycles (from ref. [21]).

3.4. *In-situ* TEM of Al Lithiation

In contrast to Si and Ge, Al has infrequently been used as an anode for LIBs due to its observed capacity being significantly lower than the theoretical value, ~ 993 mAh/g. We performed *in-situ* TEM investigations of Al NWs in order to understand the lithiation mechanisms and low capacity observed for this material.[22] The lithiation mechanism of Al NWs was found to be distinctly different than that of Si and Ge. Specifically, Al has a native oxide of Al_2O_3 that coats its surface. During lithiation, this Al_2O_3 reacts with Li to form a glassy phase of nominal composition, $LiAlO_2$ (the thermodynamically-expected phase). Once formed, $LiAlO_2$ is stable and does not undergo delithiation. As a result, the $LiAlO_2$ layer remains as a shell while the Al beneath undergoes alloying with lithium. Following delithiation, the Li_xAl alloy reverts to Al and the formation of nanoscale voids, see Figure 8. After several cycles, the Al islands become discontinuous and lose electrical contact with their neighbors (pulverization). The low capacity for Al is a result of two processes: some Li is lost during the conversion of Al_2O_3 to $LiAlO_2$, and some Al is lost during the pulverization process.

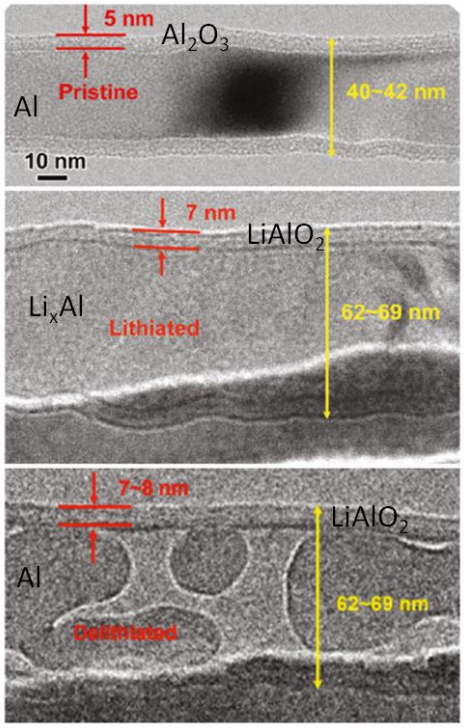

Figure 8. After a few cycles of lithiation-delithiation, Al NWs exhibit a morphology of isolated Al islands surrounded by a glassy $LiAlO_2$ shell (from ref. [22]).

3.5. *In-situ* TEM of ZnO Lithiation

ZnO is another conversion anode material for LIBs similar to SnO_2, but the process of lithiation of ZnO is markedly different than SnO_2. We examined the lithiation mechanism and defect structure in ZnO NWs using *in-situ* TEM electrochemistry.[23] In contrast to SnO_2, we observed that lithiation of ZnO proceeds by the formation of nanocracks ahead of the lithiation front, see Figure 9. Li^+ diffusion along the nanocracks was rapid, leading to amorphization of the crack interfaces. The nanocracks merged, creating an amorphous zone comprised of nanodomains of amorphized reacted material. This lithiation process proceeded without dislocation nucleation, in contrast to SnO_2. From model calculations, we suggest that crack initiation in ZnO is the result of a lithium embrittlement mechanism, which is not observed for SnO_2.

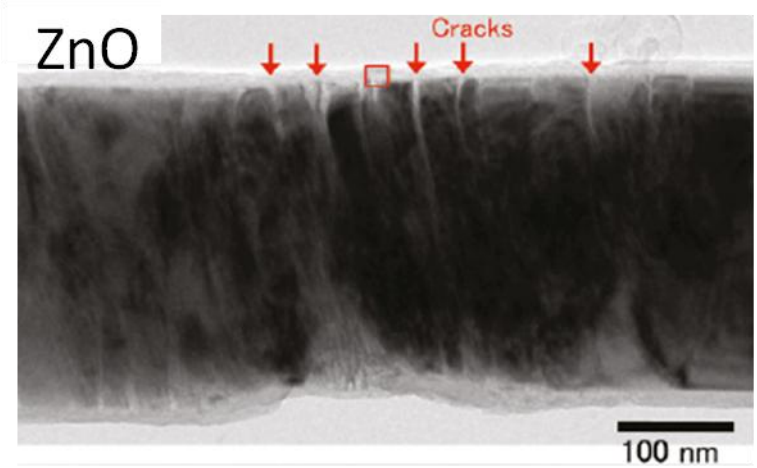

Figure 9. The lithiation of ZnO leads to the formation of nanocracks ahead of the reaction front. Amorphization occurs along the cracks, which eventually merge to form a fully amorphous region (from ref. [23]).

3.6. Other *In-situ* TEM Studies

A summary of some of our studies of *in-situ* TEM electrochemistry of anode materials for LIBs is reported in a perspective article in the journal of Energy and Environmental Science.[24] In addition to the studies on anode wires, we have also observed lithiation-induced embrittlement of multi-wall carbon nanotubes (MWCNT).[25] This embrittlement leads to an unusual fracture mechanism of the MWCNTs where pure brittle fracture is observed with sharp edges, unlike the intertube sliding fracture observed in pristine MWCNTs. Finally, we also observed lithium plating inside the TEM wherein Li fibers were observed to nucleate and grow in IL electrolytes from NW anodes, such as SnO_2.[26] These Li fibers are reminiscent of the Li dendrites that form during electroplating and that have hindered the development of reversible Li metal batteries.

4. *IN-SITU* TEM PLATFORMS

A significant portion of effort in this project was directed towards the creation of new *in-situ* TEM platforms that enable the study of nanomaterials for LIBs and the study of processes at the electrode/electrolyte interfaces. In this section, we describe our efforts to create two *in-situ* TEM platforms, a MEMS-based platform for performing *in-situ* TEM electrochemistry using volatile electrolytes, such as ethylene carbonate-based electrolytes, and a multi-electrode platform that is optimal for performing single nanowire electrochemistry combined with electrical characterization and TEM structure characterization. Some of this work has been appeared in publications[27] or has been submitted[28]. In addition, we report details of the design and fabrication of the *in-situ* TEM liquid cell in the Appendix to this report.

4.1. Multi-electrode Platforms for *In-situ* TEM Studies

Many of the changes that occur in Li-ion battery cathode and anode materials during lithiation and delithiation do not directly depend on the nature of the electrolyte. Examples include the phase changes that occur in conversion anode materials or certain cathode materials, such as $LiMn_2O_4$.[29] These phenomena are primarily a function of the Li content of the anode or cathode. In order to investigate this behavior, we have developed platforms for *in-situ* TEM characterization that do not require the use volatile electrolytes. These platforms use multi-electrode arrays for the ready assembly of nanoscale battery materials. Futhermore, they are appropriate for electrical characterization as well as structural characterization of these materials during or following electrochemical lithiation.

In order to investigate electrochemical reactions inside a TEM, it is necessary to separate the oxidation and reduction processes through the use of an electrolyte. One approach is to use a non-volatile electrolyte. Ionic liquids are a relatively new class of liquid salts that have the advantage of high salt solubility (which enables their use as an electrolyte) and extremely low vapor pressure (which enables their use in high vacuum environments). The use of ionic liquids as Li-ion battery electrolytes has been the subject of much investigation with most attention paid to their high electrochemical stability, low flammability, and low vapor pressure.[30] For our applications, we are interested in their use as liquid electrolytes that may be used without encapsulation inside a TEM. For our studies, we used two types of ionic liquids, both of which behaved similarly: 1,2-Dimethyl-3-propylimidazolium (DMPI) with bis(trifluoromethyl-sulfonyl)imide (TFSI) and Li-TFSI salt and 1-butyl-3-methylimidazolium (BMI) with hexafluorophosphate (PF_6) and $LiPF_6$ salt. The ionic liquids may be introduced into the TEM by spin coating, drop casting, or dipping. Figure 10 shows a TEM image of a holey-carbon grid dipped into BMI-PF_6. The ionic liquid has sufficient surface tension to bridge small openings, enabling its use without substrate support, a desirable feature to minimize the sample thickness for high resolution TEM imaging.

To utilize ionic liquid electrolytes, we have developed unsealed electrochemical platforms that permit the examination of nanoscale battery materials that are assembled on to the platform by dielectrophoresis (DEP), an assembly process where particles in solution are attracted or repelled to regions of high electric field gradient generated by closely-spaced electrodes driven by AC signals. Figure 11 shows one platform design that consists of arrays of gold electrodes patterned on top of a layer of silicon nitride on top of silicon. There is a gap of 350 nm between

electrodes, and in this region the electrodes lay atop a silicon nitride membrane. Between the electrodes, the silicon nitride has been etched to create a clearance hole. DEP was then used to assemble single or multiple nanowires between the electrode pairs. The advantage of this array design is that multiple single nanowire samples may be examined all on a single chip.

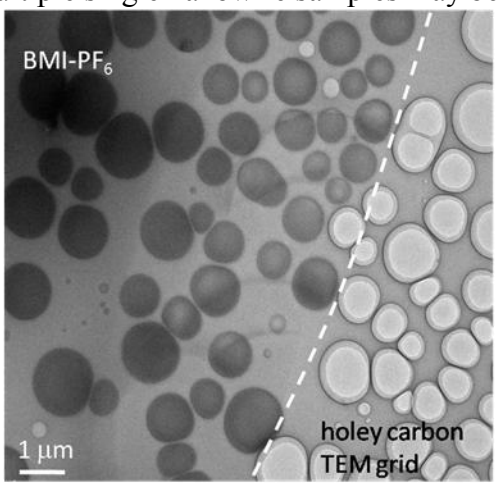

Figure 10. TEM image showing a holey carbon grid partially coated with BMI-PF6. The dashed line shows the approximate boundary between coated and uncoated regions. The ionic liquid is able to span small openings.

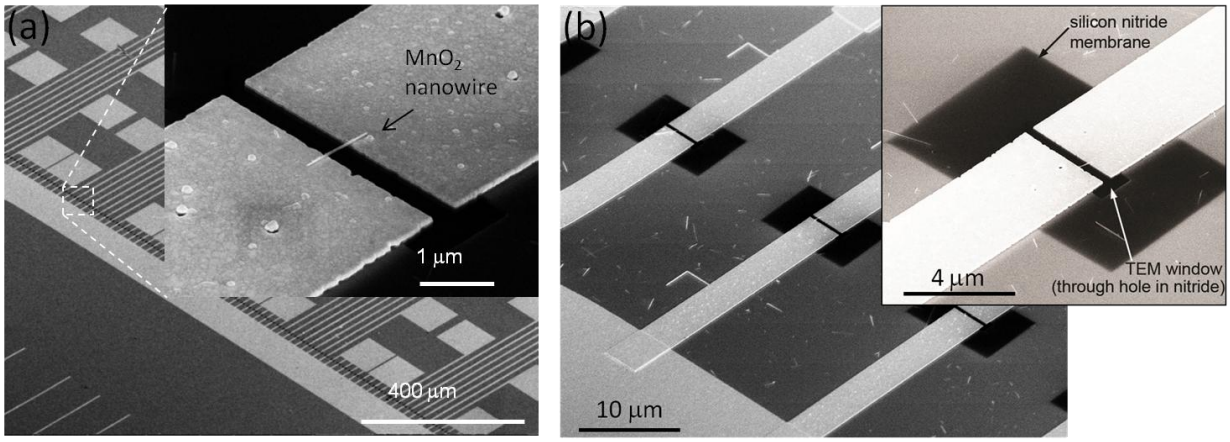

Figure 11. SEM images showing the multi-electrode platform containing a high density electrode array. A single MnO_2 nanowire assembled on the electrodes is shown in the inset in (a). The structure of the electrodes, sitting on Si_3N_4 membranes with through-holes, is shown in (b).

It is possible to perform multiple DEP assembly operations to incorporate disparate electrode materials on the same *in-situ* TEM platform. This is advantageous, for example, in order to assemble working electrode and counter electrode materials in close proximity. One example of this is the co-assembly of a Si NW anode with $LiFePO_4$ cathode nanoparticles as a counter electrode, see Figure 12.

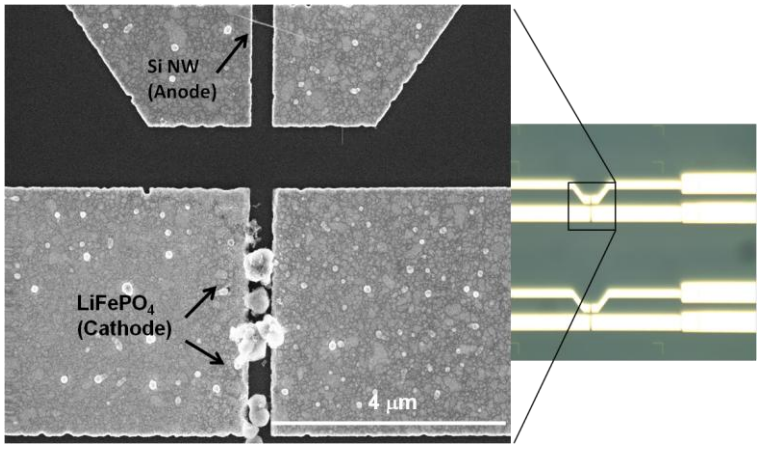

Figure 12. Example of the co-assembly of both Si NWs and $LiFePO_4$ nanoparticles using 2-step DEP on separate electrodes.

To demonstrate the use of the multi-electrode platform with a model system, we used MnO_2 nanowires which are a representative material for common Li-ion battery cathodes. MnO_2 was chosen for several reasons: 1. some Li_xMnO_2 compounds, specifically the spinel phase $Li_xMn_2O_4$, are Li-ion battery cathodes with reasonable capacity (similar to $LiCoO_2$),[30] 2. MnO_2 compounds often undergo phase transitions as a function of Li concentration, such as the cubic to tetragonal transition in $Li_xMn_2O_4$ at x=1, and this provides the opportunity to observe phase transitions by TEM;[31]; and 3. lithiated oxide cathodes tend to have good stability in air, and this was desirable for experiments where lithiation was performed in a glove box with the samples then being transferred to air. The MnO_2 nanowires were fabricated by hydrothermal synthesis following the work of Wang and Li.[32] TEM revealed the nanowires to be β-MnO_2 (tetragonal structure, $P4_2/mnm$) with typical lengths < 3 μm and typical diameters of 35 nm.

The MnO_2 nanowires were assembled on to the unsealed electrochemical platforms by DEP. First, the nanowires were suspended in ethanol and dispersed by sonication. They were then assembled on to the chips using DEP with a frequency of 1 kHz and voltages of 1 to 2 V. Following assembly, the chips were rinsed in clean ethanol and dried in flowing $N_{2(g)}$.

Lithiation of the nanowires was performed in a He-filled glove box using a Li metal foil as a counter and reference electrode and using EC/DMC (1:1) - 1 M $LiPF_6$ electrolyte. Contact to the electrodes on the chip was made using Au-tipped needles from a probe station placed inside the glove box. Using large dispersions of MnO_2 nanowires on a separate sample, typical open circuit voltages of around 3.3 V were observed. Using this value of open circuit voltage, the isolated nanowires were lithiated by a slow potentiodynamic scan from 3.3 V to 1.5 V. Due to the very small mass of the nanowires, the discharge current during lithiation that arises solely from the nanowires could not be measured; thus potential control was used to control lithium content. Based on Thackeray's work with β -MnO_2, 1.5 V should be sufficient to fully lithiate this material with the expected Li loading ranging from $Li_{x=0.2}MnO_2$ to $Li_{x=0.7}MnO_2$ for highly crystalline to highly disordered structures, respectively.[33]

The electrochemical platform has electrical contacts to both sides of the nanowire, permitting electrical characterization of the nanowires before and after lithiation. This is an advantage for battery materials' characterization at the single particle level. Specifically, one can distinguish changes in electrode impedance due to changes in the electronic conductance of the materials

themselves, i.e. changes in electrical conductivity of individual nanowires, versus changes in electronic conductance between particles, i.e. interfacial impedance. These platforms enable measurement of the intraparticle electronic conductance whereas measurements on mats of nanowires include both intraparticle and interfacial electronic conductances. The electronic conductance of the MnO_2 nanowires was measured prior to and following lithiation using 2-point measurements at the Au contact pads. Figure 13 shows a representative result, where a large decrease in electronic conductance is observed following lithiation. Such behavior may be expected in view of the dilation of the lattice following Li insertion and the known metal-insulator transition that can occur in similar oxide materials following lattice expansion,[34] or the low electronic conductance might originate from the high lattice disorder observed by TEM (see below).

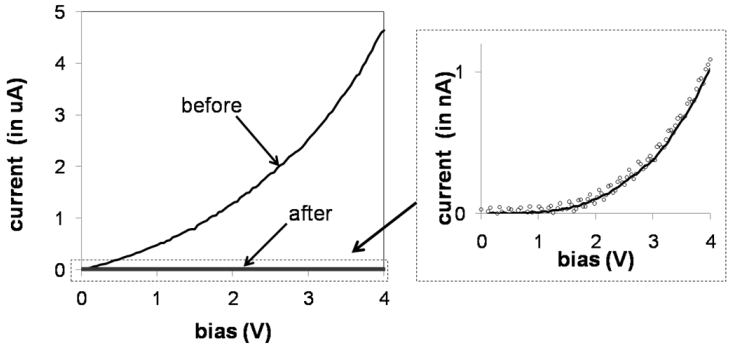

Figure 13. Current-voltage characterization of an individual MnO_2 nanowire before and after lithiation.

Structural characterization of the MnO_2 nanowires was performed using TEM on representative nanowires before and after lithiation. Figure 14 shows high resolution TEM images indicating the high crystallinity of the nanowires prior to lithiation and the high lattice disorder following lithiation. Despite the high defect density of the lithiated wire, the structure was still β-phase as determined by electron diffraction. The observation that these NWs do not undergo a phase transformation despite Li-loading concentrations approaching $Li_{0.5}MnO_2$ is consistent with observations of Jiao and Bruce that showed mesoporous β-MnO_2 remains single phase up to $Li_{0.9}MnO_2$.[35]

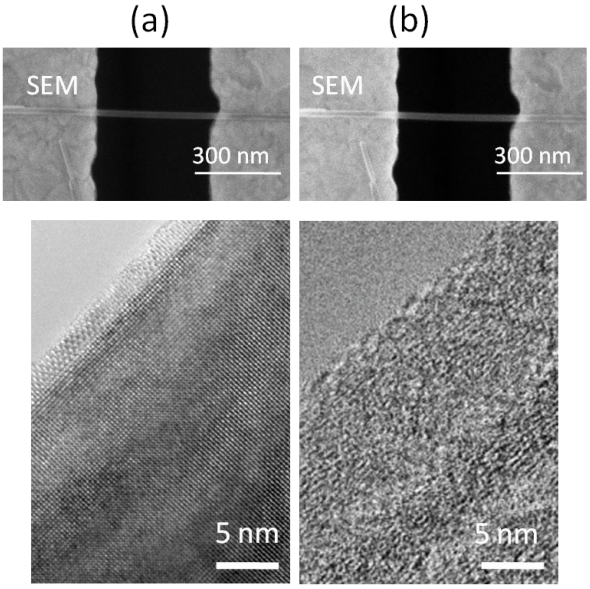

Figure 14. SEM (top) and TEM (bottom) images of representative MnO_2 nanowires (a) before and (b) after lithiation.

4.2. *In-situ* TEM Liquid Cell

In section 2, we noted the importance of electrochemical reactions at the electrode/electrolyte interface involving the reduction of EC and the formation of the SEI. Our goal is to observe these electrode/electrolyte reactions and SEI formation inside the TEM, but one of the greatest challenges in performing liquid electrochemistry inside a TEM is introducing volatile electrolytes into the high vacuum of the TEM sample chamber, typically 10^{-5} Torr or better.[36] For example, many commercially-available carbonate-based Li-ion battery electrolytes use diethyl carbonate (DEC) or dimethyl carbonate (DMC), typically mixed with ethylene carbonate (EC), and these liquids have vapor pressures of 10 to 18 Torr at room temperature. One approach for introducing volatile liquids is to seal the liquid inside a narrow channel that is thin enough to permit electron transmission. Encapsulation of a liquid inside a TEM has been achieved before in a few isolated cases. One of the first of these TEM liquid cells was created by Williamson, *et al.*, for the study of Cu electrodeposition during TEM imaging.[37,38] This platform used two silicon chips with thin silicon nitride membranes assembled face-to-face, sealing in an aqueous electrolyte. Several other designs based on this flip-chip approach have been pursued by other investigators using membranes of silicon nitride, silicon dioxide, or polymer and for studies ranging from imaging of cells in solution to nanoparticle synthesis.[39-42]

With a focus on developing a versatile electrochemical cell that is TEM-compatible and that permits high resolution imaging, we have used micro-electromechanical systems (MEMS) fabrication processes to create a platform with multiple electrical and insulating layers. Our design utilizes ultra-thin silicon nitride windows that are less than 40 nm thick in order to reduce electron absorption during TEM imaging. This approach, however, requires small diameter nitride windows (approximately 20 microns to less than 5 microns across), and this complicates the alignment of the top and bottom chips. Our design incorporates unique features to solve this issue, including alignment features that promote precise X-Y alignment and electrical interconnects that are buried beneath silicon nitride. A simplified schematic of the platform is shown in Figure 15.

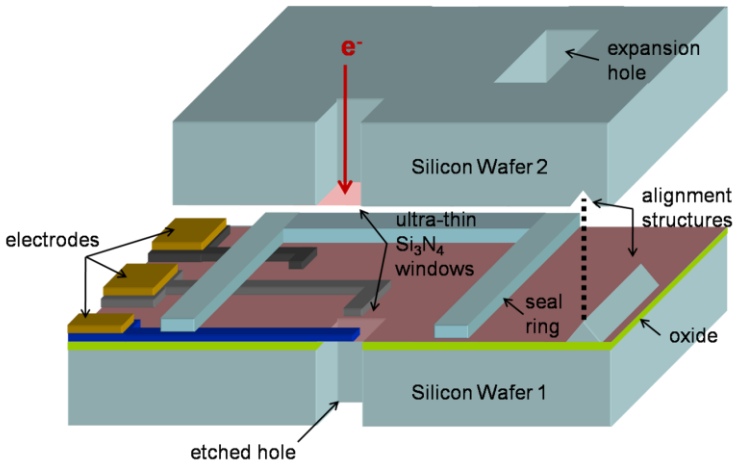

Figure 15. Schematic of the electrochemical platform for TEM imaging. In the fabricated structure, the electrodes are buried beneath silicon nitride and silicon dioxide up to the region immediately surrounding the silicon nitride window.

The alignment structure uses pyramidal pits that are etched to accept to accept sapphire micro-lenses, see Figure 16. The electrodes have a design structure consisting of a buried doped polycrystalline silicon interconnect that is covered by 0.5 μm of SiO_2, see Figure 17. At the contact pads and near the silicon nitride window, additional metallization is applied, either Al, TiN, or W (70 nm thick), and these connect to the buried interconnect through a via in the silicon nitride and SiO_2. The interconnect itself passes beneath a raised polycrystalline seal ring that is 1000 nm high. The seal ring minus the raised mesa height on the mating chip (900 nm) serves to fix the gap between the top and bottom chips, defining the thickness of the liquid channel, ~ 100 nm in this design. The top and bottom chips are sealed by a low viscosity epoxy that wicks along the raised seal ring.[43]

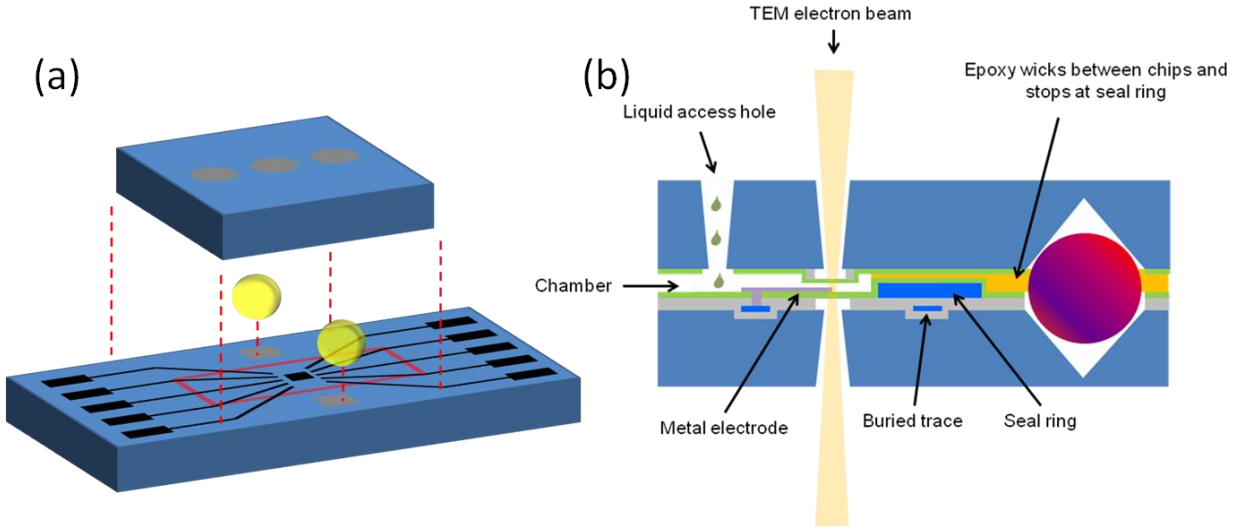

Figure 16. Schematic of the cross-section of the *in-situ* TEM liquid cell showing the alignment structures based on pyramidal pits that contact a sapphire microlens.

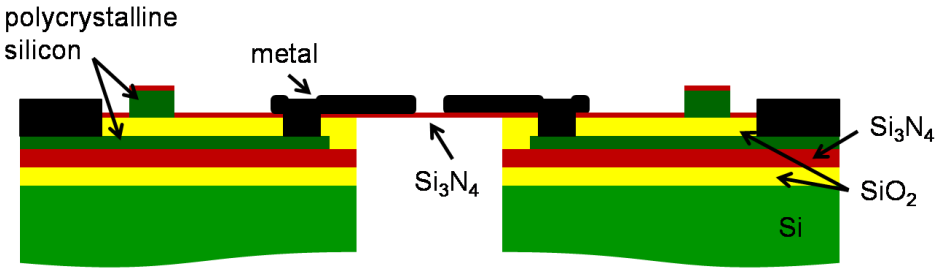

Figure 17. Schematic of the cross-section of the bottom chip showing the buried electrical interconnects.

Numerous electrode configurations for the bottom chip were designed (a total of twenty variants, ranging from as few as 4 electrodes up to 10 electrodes). See Figure 18 for one set of designs. We designed the electrodes to permit the incorporation of electroactive material by electroplating, e.g electrodeposition of Li metal, or by directed assembly of nanoscale or micro-scale particles. We use dielectrophoresis (DEP) to assemble these materials. Two examples are shown in Figure 19.

Figure 20 shows the assembled *in-situ* TEM liquid cell mounted on to a TEM holder and a TEM image looking through the TEM liquid cell that has been filled with an EC-DEC Li-ion battery electrolyte. Electrochemical testing using the *in-situ* TEM liquid cell is currently in progress.

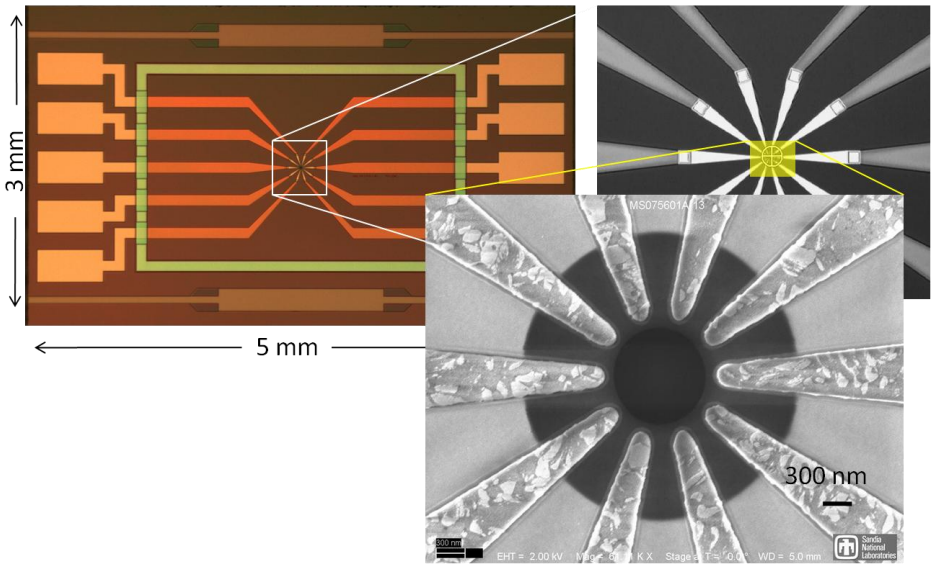

Figure 18. Optical microscope image (upper left) and scanning electron microscope (SEM) images of the bottom chip showing one of the twenty electrode configurations.

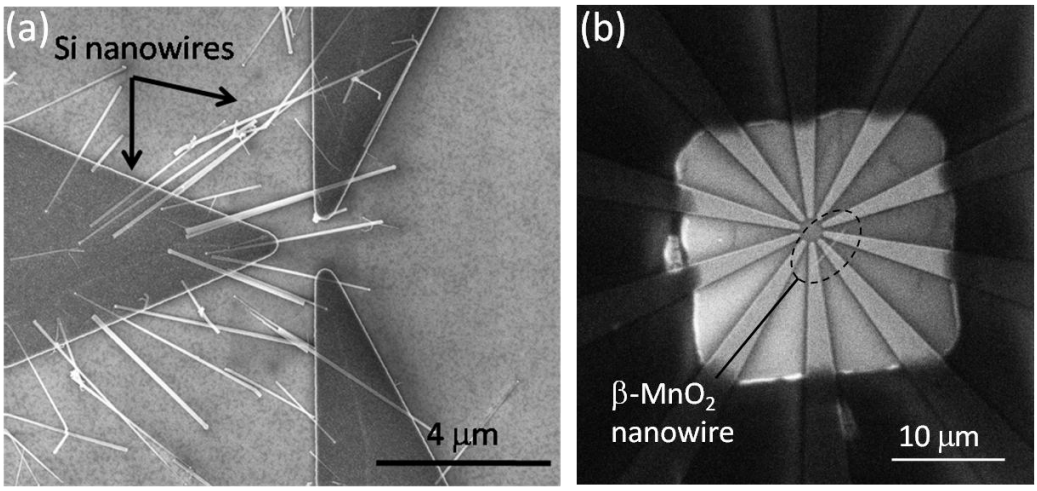

Figure 19. SEM images showing the DEP assembly of (a) silicon nanowires and (b) a MnO_2 nanowire on to two different electrode configurations of the platform.

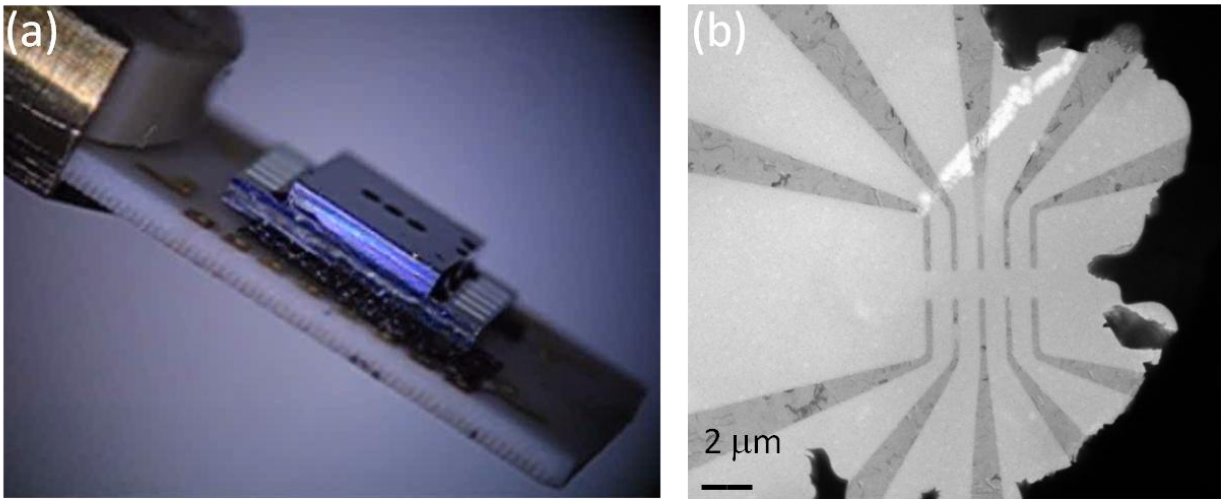

Figure 20. (a) *In-situ* TEM liquid cell mounted on to TEM holder. (b) TEM imaging through the *in-situ* TEM liquid cell after filling with EC-DEC battery electrolyte.

4.3. Summary and Conclusions

This work has focused on the development of electrochemical platforms that are suitable for the *in-situ* characterization of Li-ion battery materials by TEM. Two types of platforms have been developed: a multi-electrode platform designed for the assembly and electrical testing of a large number of isolated nanowires and a MEMS-fabricated *in-situ* TEM liquid cell platform that provides encapsulation of electrolytes. The multi-electrode platform used arrays of closely-spaced electrodes for the DEP assembly of battery materials. Ionic liquid electrolytes provided a means of using an electrolyte inside a TEM without encapsulation. These were found to be entirely vacuum compatible and easy to apply. As a model system to test features of the unsealed platform, MnO_2 nanowires were assembled by DEP across electrodes of the platform, and electrochemical testing was performed. These nanowires were lithiated outside the TEM using conventional ethylene carbonate-based electrolytes inside a glove box. Imaging of the nanowires before and after lithiation revealed that the nanowires remained in their original β-phase, but the defect density and lattice disorder was greatly increased. The MEMS platform used flip-chip assembly and special alignment features to create precision alignment of top and bottom chips. Multiple electrode configurations were created to permit the assembly using dielectrophoresis (DEP) of nanoscale or micro-scale battery materials in the region of interest. These preliminary experiments establish the framework for the complete *in-situ* characterization of battery materials, where processes such as SEI formation during lithiation may be viewed in real-time with atomic-scale resolution.

5. REFERENCES

1. see "USABC Goals for Advanced Batteries for EVs," http://www.uscar.org/guest/article_view.php?articles_id=85.
2. Nagaura, T. and Tozawa, K., "Lithium ion rechargeable battery," Prog. Batteries Solar Cells **9**, 209 (1990).
3. Note that the USABC goals for specific energy are for a complete battery pack *module*, and this would require specific energies *per cell* probably substantially greater than 150 Wh/kg.
4. Tarascon, J.-M. and Armand, M., "Issues and challenges facing rechargeable lithium batteries," Nature **414**, 359 (2001).
5. Arico, S. A., Bruce, P, Scrosati, B., Tarascon, J.-M., and van Schalkwijk, W. "Nanostructured materials for advanced energy conversion and storage devices," Nature Mater. **4**, 366 (2005).
6. Aurbach, D., "Surface Films in Lithium-Ion Batteries," in Advances in Lithium-Ion Batteries, pp. 7-77, van Schalkwijk, W. A. and Scrosati, B. eds. (Kluwer Academic, New York, 2002).
7. Aurbach, D., Makovsky, B., Levi, M. D., Levi, E., Schechter, A., Moshkovich, M., and Cohen, Y., J. Power Sources **81-82**, 95 (1999).
8. Broussely, M., "Aging mechanisms and calendar-life predictions in lithium-ion batteries," in Advances in Lithium-Ion Batteries, pp. 393-432, van Schalkwijk, W. A. and Scrosati, B. eds. (Kluwer Academic, New York, 2002).
9. Chan, C. K., Peng, H., Liu, G., McIlwrath, K., Zhang, X. F., Huggins, R. A., and Cui, Y., "High-performance lithium battery anodes using silicon nanowires," Nature Nanotech. **3**, 31 (2008).
10. Graetz, J., Ahn, C. C., Yazami, R., and Fultz, B., "Highly reversible lithium storage in nanostructured silicon," Electrochem. Solid-State Lett. **6**, A194 (2003).
11. Chung, S.-Y., Bloking, J. T., and Chiang, Y.-M., "Electronically conductive phospho-olivines as lithium storage electrodes," Nature Mater. **1**, 123 (2002).
12. Shao-Horn, Y., "Understanding phase transformations in lithium battery materials by transmission electron microscopy," in Lithium Batteries: Science and Technology, pp. 478-506, Nazri, G.-A. and Pistoia, G. eds. (Springer, New York, 2009).
13. Leung, K and Budzien, J. L., "Ab initio Molecular Dynamics simulations of the initial stages of solid-electrolyte interphase formation on lithium ion battery graphitic anodes," Physical Chem. Chem. Physics **12**, 6583 (2010).*
14. Yu, J., Balbuena, P. B., Budzien, J., and Leung, K, "Hybrid DFT Functional-Based Static and Molecular Dynamics Studies of Excess Electron in Liquid Ethylene Carbonate," J. Electrochem. Soc. **158**, A400 (2011).*
15. Leung, K., Qi, Y., Zavadil, K. R., Jung, Y. S., Dillon, A. C., Cavanagh, A. S., Lee, S.-H. and George, S. M., "Using atomic layer deposition to hinder solvent decomposition in lithium ion batteries: first principles and experimental studies," J. Am. Chem. Soc. **133**, 14741 (2011).*
16. Huang, J. Y., Zhong, L., Wang, C. M., Sullivan, J. P., Xu, W., Zhang, L. Q., Mao, S. X., Hudak, N. S., Liu, X. H., Subramanian, A., Fan, H. Y., Qi, L., Kushima, A., and Li, J., "In-situ observation of the electrochemical lithiation of a single SnO_2 nanowire electrode," Science **330**, 1515 (2010).*

17. Zhong, L., Liu, X. H., Wang, C. M., Wang, G. F., Mao, S. X., and Huang, J. Y., "Multiple-stripe lithiation mechanism of individual SnO_2 nanowires in a flooding geometry," Phys. Rev. Lett. **106**, 248302 (2011).*
18. Zhang, L. Q., Liu, X. H., Liu, Y., Huang, S., Zhu, T., Gui, L., Mao, S. X., Ye, Z. Z., Wang, C. M., Sullivan, J. P., and Huang, J. Y., "Controlling the Lithiation Induced Strain and Charging Rate in Nanowire Electrodes by Coating," ACS Nano **5**, 4800 (2011).*
19. Liu, X. H., Zheng, H., Zhong, L., Huang, S., Karki, K., Zhang, L. Q., Liu, Y., Kushima, A., Liang, W. T., Wang, J. W., Cho, J.-H., Epstein, E., Picraux, S. T., Zhu, T., Li, J., Sullivan, J. P., Cumings, J., Wang, C., Mao, S. X., Ye, Z. Z., Zhang, S., and Huang, J. Y., "Anisotropic swelling and fracture of silicon nanowires during lithiation," Nano Lett. **11**, 3312 (2011).*
20. Liu, X. H., Zhang, L. Q., Zhong, L., Liu, Y., Zheng, H., Wang, J. W., Cho, J.-H., Dayeh, S. A., Picraux, S. T., Sullivan, J. P., Mao, S. X., Ye, Z. Z., and Huang, J. Y., "Ultrafast electrochemical lithiation of individual Si nanowire anodes," Nano Lett. **11**, 2251, (2011).*
21. Liu, X. H., Huang, S., Picraux, S., Li, J., Zhu, T., and Huang, J. Y., "Reversible nanopore formation in Ge nanowires during lithiation-delithiation cycles: an in situ TEM study," Nano Lett. **11**, 3991 (2011).*
22. Liu, Y., Hudak, N. S., Huber, D. L., Limmer, S. J., Yelton, W. G., Sullivan, J. P., and Huang, J. Y., "In situ TEM observation of pulverization of aluminum nanowires and evolution of the thin surface Al_2O_3 layers during lithiation-delithiation cycles," Nano Lett. **11**, 4188 (2011).*
23. Kushima, A., Liu, X. H., Zhu, G., Li, J., Wang, Z. L., and Huang, J. Y., "Leapfrog cracking and nanoamorphization of ZnO nanowire during in-situ electrochemical lithiation," Nano Lett. **11**, 4535 (2011).*
24. Liu, X. H., and Huang, J. Y., "*In situ* TEM electrochemistry of anode materials in lithium ion batteries," Energy Environ. Sci. **4**, 3844 (2011).*
25. Liu, Y., Zheng, H., Liu, X. H., Huang, S., Zhu, T., Wang, J. W., Kushima, A., Hudak, N. S., Huang, X., Zhang, S. L., Mao, S. X., Qian, X. F., Li, J., and Huang, J. Y., "Lithiation induced embrittlement of multi-walled carbon nanotubes," ACS Nano **5**, 7245 (2011).*
26. Liu, X. H., Zhong, L., Zhang, L. Q., Kushima, A., Mao, S. X., Li, J., Ye, Z. Z., Sullivan, J. P., and Huang, J. Y. "Lithium fiber growth on the anode in a nanowire lithium ion battery during charging," Appl. Phys. Lett. **98**, 183107 (2011).*
27. Sullivan, J. P., Huang, J., Shaw, M. J., Subramanian, A., Hudak, N., Zhan, Y., and Lou, J., "Understanding Li-ion battery processes at the atomic to nano-scale," Proc. of SPIE **7683**, 76830B1 (2010).*
28. Subramanian, A., Sullivan, J. P., Huang, J. Y., Hudak, N., Zhan, Y., and Lou, J., "Single nanowire structural, electrical, and electrochemical characterization during lithium insertion," (Submitted 2011).*
29. Thackeray, M. M., "Manganese oxides for lithium batteries," Prog. Solid St. Chem. **25**, 1 (1997).
30. Webber, A. and Blomgren, G. E., "Ionic liquids for lithium ion and related batteries," pp 185-232 in Advances in Lithium-Ion Batteries, van Schalkwijk, W. A. and Scrosati, B. eds. (Kluwer, New York, 2002).
31. Thackeray, M. M., Shao-Horn, Y., Kahaian, A. J., Kepler, K. D., Skinner, E., Vaughey, J. T., and Hackney, S. A., "Structural fatigue in spinel electrodes in high voltage (4 V) Li/LixMn_2O_4 cells," Electrochem. Solid-State Lett. **1**, 7 (1998).
32. Wang, X. and Li, Y., "Selected-control hydrothermal synthesis of α- and β- MnO_2 single crystal nanowires," J. Am. Chem. Soc. **124**, 2880 (2002).

33. Thackeray, M. M., de Kock, A., de Picciotto, L. A., and Pistoia, G., "Synthesis and characterization of β-MnO_2 from $LiMn_2O_4$," J. Power Sources **26**, 355 (1989).
34. Goodenough, J. B., in Progress in Solid State Chemistry, Vol. 5, Reiss, H. ed. (Pergamon Press, Oxford, 1971).
35. Jiao, F., and Bruce, P. G., "Mesoporous crystalline β-MnO_2 – a reversible positive electrode for rechargeable lithium batteries," Adv. Mater. **19**, 657 (2007).
36. New-generation environmental TEMs permit pressures at the sample up to 10 Torr, for example, see Hoffman, S., Sharma, R., Wirth, C. T., Cervantes-Sodi, F., Ducati, C., Kasama, T., Dunin-Borkowski, R. E., Drucker, J., Bennett, P., and Robertson, J., "Ledge-flow-controlled catalyst interface dynamics during Si nanowire growth," Nature Mater. **7**, 372 (2008).
37. Williamson, M. J., Tromp, R. M., Vereecken, P. M., Hull, R., and Ross, F. M., "Dynamic microscopy of nanoscale cluster growth at the solid-liquid interface," Nature Mater. **2**, 532 (2003).
38. Ross, F. M., "Growth processes and phase transformations studied by in situ transmission electron microscopy," IBM J. Res. Develop. **44**, 489 (2000).
39. Thiberge, S., Nechushtan, A., Sprinzak, D., Gileadi, O., Behar, V., Zik, O., Chowers, Y., Michaeli, S., Schlessinger, J., and Moses, E., "Scanning electron microscopy of cells and tissues under fully hydrated conditions," Proc. Natl. Acad. Sci. **101**, 3346 (2004).
40. Liu, K.-L., Wu, C.-C., Huang, Y.-J., Peng, H.-L., Chang, H.-Y., Chang, P., Hsu, L., and Yew, T.-R., "Novel microchip for in situ TEM imaging of living organisms and bio-reactions in aqueous conditions," Lab Chip **8**, 1915 (2008).
41. de Jong, N., Peckys, D. B., Kremers, G. J., and Piston, D. W., "Electron microscopy of whole cells in liquid with nanometer resolution," Proc. Natl. Acad. Sci. **106**, 2159 (2009).
42. Zheng, H., Smith, R. K., Jun, Y.-W., Kisielowski, C., Dahmen, U., and Alivisatos, A. P., "Observation of single colloidal platinum nanocrystal growth trajectories," Science **324**, 1309 (2009).
43. We have used Epotec 310 epoxy.

** = publications performed in this LDRD project*

APPENDIX A: DESIGN AND FABRICATION OF THE *IN-SITU* TEM LIQUID CELL

Fabrication

The sealed micro machined silicon chamber that can be used to view electrochemistry *in-situ* with a TEM (Transmission Electron Microscope) was designed to fit into a TEM chamber and has electrodes that extend into a small viewing window made of very thin silicon nitride. Exterior bond pads give access to the internal electrode set. The platform top and bottom are self aligned with a unique anisotropic KOH etch strategy in combination with sapphire or ruby ball lenses, making assembly very easy with common lab equipment. The chamber can be assembled after depositing materials on the electrodes or can be assembled and have material such as electrolyte introduced into the chamber through 2 access holes which can be sealed with vacuum grease or other sealant. Figure A1 shows an image of a completed Prototype 1 platform bottom.

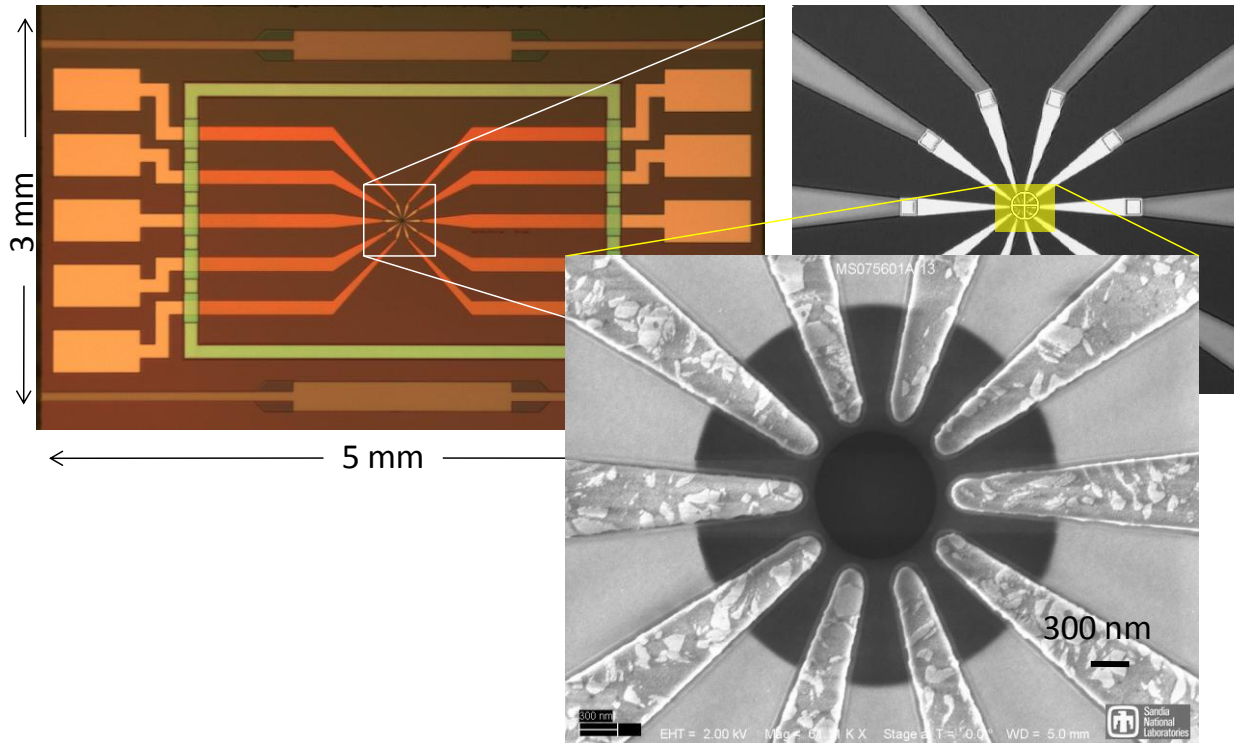

Figure A1. Bottom chip of *in-situ* TEM Platform, Prototype 1, showing the 10 metal electrodes over a silicon nitride film (Nitride). In this example there is a 1.0 um hole purposely etched in the center of the Nitride film to hold a fluid sample.

The bottom section of the device has bond pads and electrical traces that pass under a raised seal ring. At the center of the chamber there are metal traces that converge on a thin silicon nitride window.

The top chip of the chamber has a flat surface that rests on the seal ring and a similar nitride window and Bosch etched hole to allow the electron beam access to the thin nitride window and into the chamber. An assembled device can be seen in Figure A2.

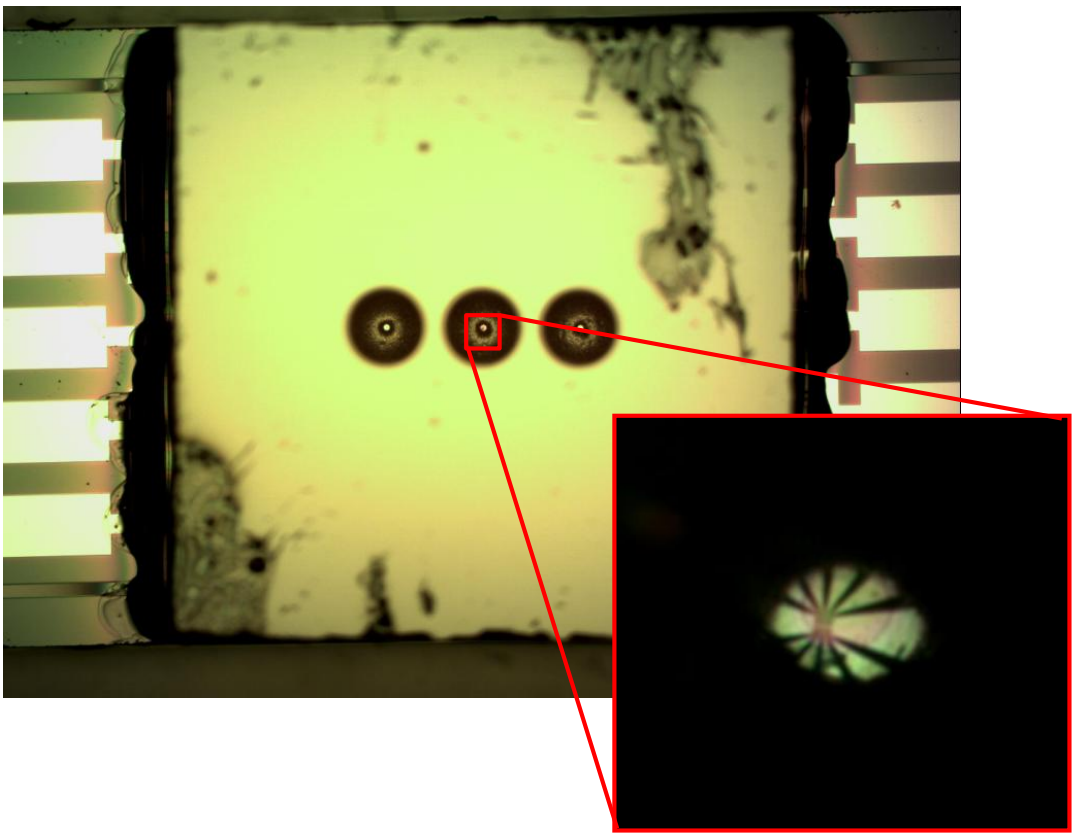

Figure A2. Prototype 1 *In-situ* TEM platform (assembled). The inset shows the electrode array as viewed from the top of the platform.

In order to keep epoxy from leaking past the seal ring and into the chamber, a force applied to the center of the top chip of 5 Newtons was required. The 5 N force was applied to the assemblies with the use of anodic bonder equipment on Prototype 1 assembly while epoxy was flowed into the gap between the chips. The Anodic bonder setup can be seen in Figure A3.

Figure A3. Anodic Bonder setup used to assemble Prototype 1 In-situ TEM chips.

The completed device shown in Figure A2 is not the final edition of the device and modifications have been made to the alignment strategy in a new design, Prototype 2. The KOH anisotropic etch that was used to create the alignment features in Prototype 1 were not deep enough to adequately find the features when sliding the parts together, also the KOH etching of the protruding features in the top chip proved to be highly variable depending on the exact alignment of the pattern to the wafer substrate crystal plane, therefore a new strategy was employed on the Prototype 2.

In Prototype 2 the KOH etch creates two inverse pyramid shaped facets that allow 600 um ball lenses to reside in the bottom chip feature. The top has a similar feature that facilitates the accurate alignment of the two electron beam holes at the center of the chip. Figure A4 shows a completed Prototype 2 bottom chip.

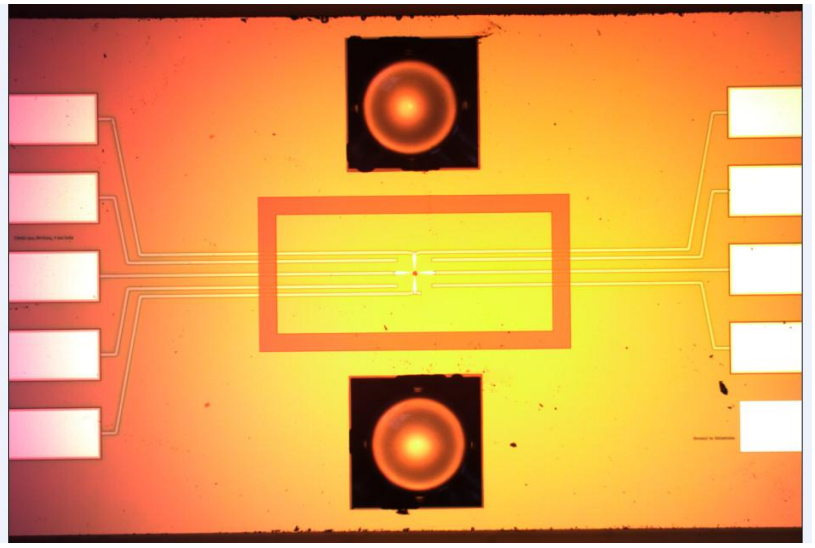

Figure A4. Prototype 2 completed bottom chip shown with 600 um ball lenses seated in the KOH etched facets.

Prototype 2 has several improvements in design to mitigate issues encountered with the Prototype 1 devices. The chamber inside the seal ring section is much smaller to allow the real estate for the ball lens facets and to reduce the area of contact between the ring and top. An image of a top chip can be seen in Figure A5.

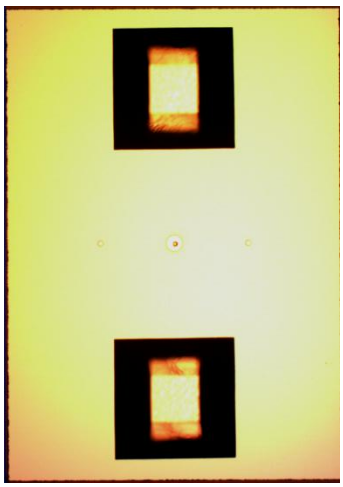

Figure A5. - Prototype 2 completed Top chip showing the ball lens facets and the TEM window at the center.

Figure A6 shows an assembled top and bottom chip with a section area showing through light passing through both pieces.

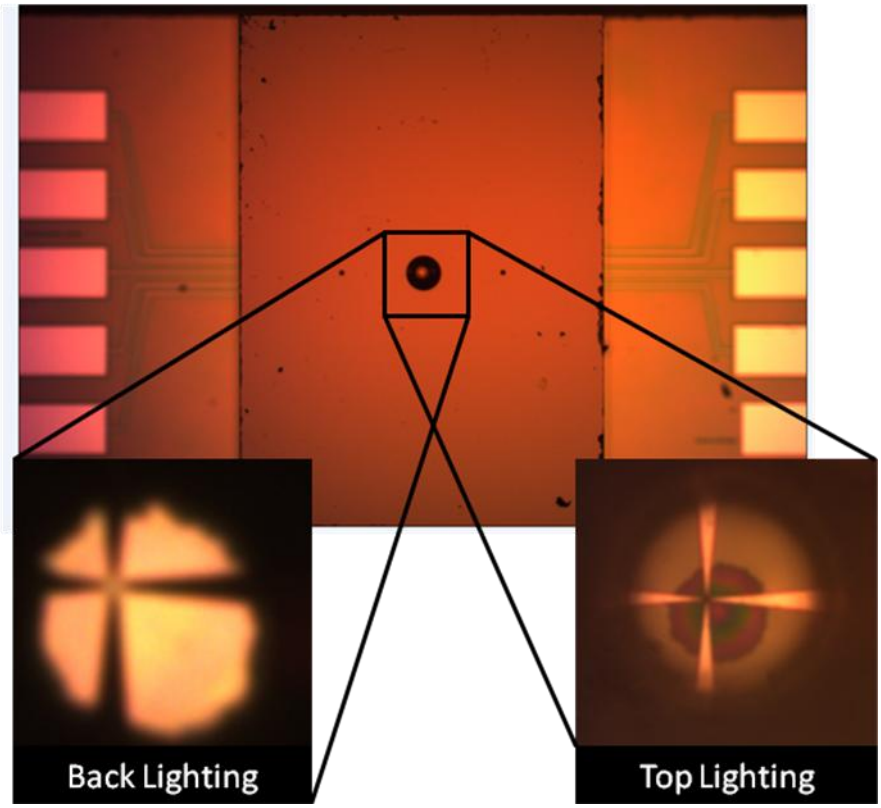

Figure A6. Assembled top and bottom chips with insets showing through holes and electrodes with both front and back side lighting.

Assembly of the chips is accomplished by use of modified plastic forceps shown in Figure A7. A sapphire ball lens is positioned over the back of the top chip so as to apply a central pressure point and then the assembly is squeezed together with the forceps. Once the chips have been assembled and passively aligned with the ball lenses, pressure is applied with an additional set of forceps and drops of epoxy are applied to the outside edges of the lid allowing the adhesive to wick between the two chips, stopping at the seal ring.

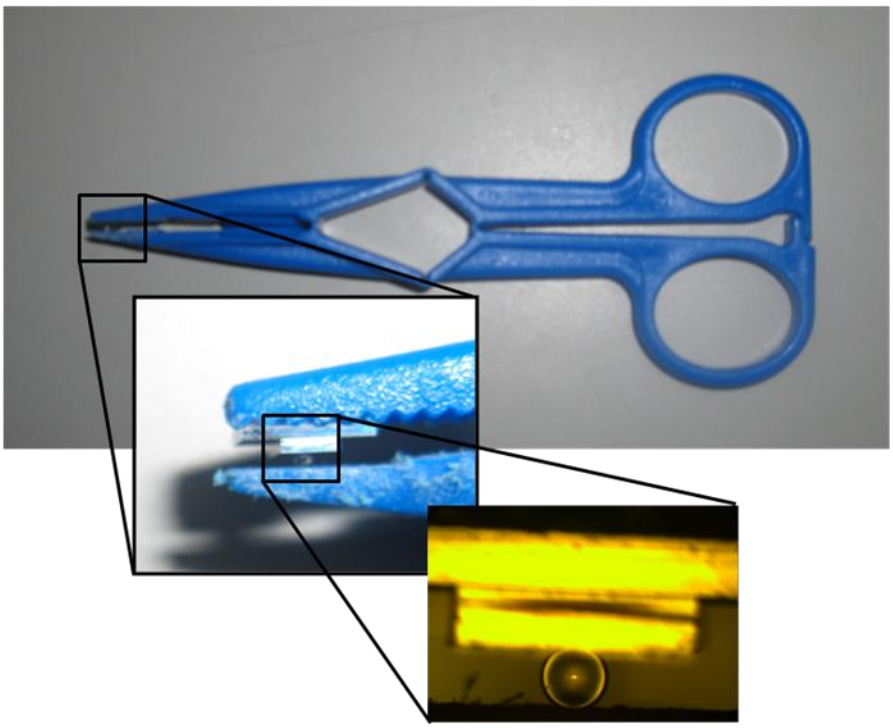

Figure A7. Modified forceps for applying force to the chips during assembly. A ball lens can be seen on the bottom jaw which resides in the center Bosch hole and distributes the pressure exactly in the center of the chamber section.

Prototype 2 also has a modification in the seal ring and lid section. In Prototype 1 we experimented with several seal ring heights to determine what height was needed to keep the epoxy from wicking into the chamber. It was found that a ring height of 1.0 um was needed in order to keep adhesive from leaking into the chamber. This posed a problem because the ideal chamber gap was 100 nm and a 1.0 um gap would be too thick for efficient electron transmission during TEM imaging. The solution was to incorporate a mesa region in the lid section that protrudes by 900 nm and is covered with the nitride film, allowing the gap to be 100 nm while keeping the seal ring 1.0 um high. This proved to be successful and a typical result can be seen in Figure A8. Experiments were carried out with two different epoxies Epotek 301, and Epotek 310 which had viscosities of 100 – 200 cPs and 1,800 - 3,300 cPs respectively. These epoxies were selected because they are room temperature curable and had viscosities that fit this application. Prototype 2 had better performance with the Epotek 310 epoxy, which flowed more completely between the top and bottom and did not seep into the chamber region.

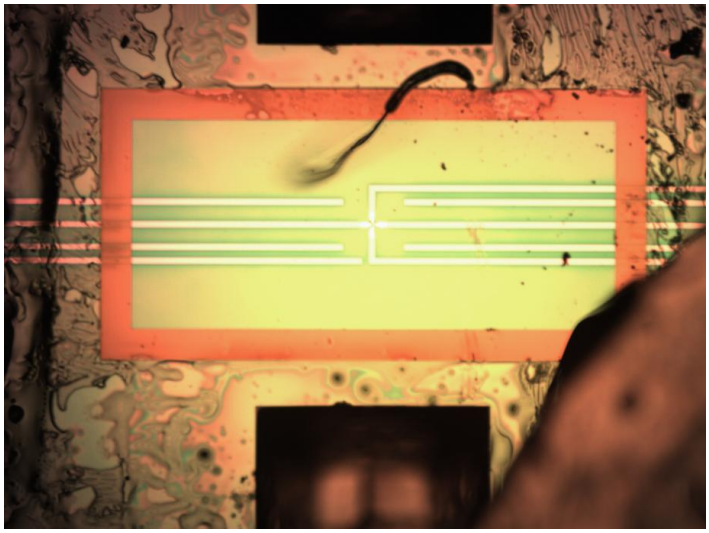

Figure A8. Disassembled bottom section of TEM chip prior to epoxy (EPOTEK 310) setting completely. No epoxy has seeped into the chamber but has wicked completely around the exterior of the ring.

While other methods of applying pressure to the lid of the TEM prototype 2 chip assemblies are surely conceivable, the forceps method was easy to implement and was the best choice for expediency purposes. In practice a jig could easily be constructed that would hold the bottom and top in place while applying pressure to the top chip in the center of the chamber.
The fabrication process flow for the Ball Lens alignment approach (Prototype 2) can be found in Figures A9 through A13.

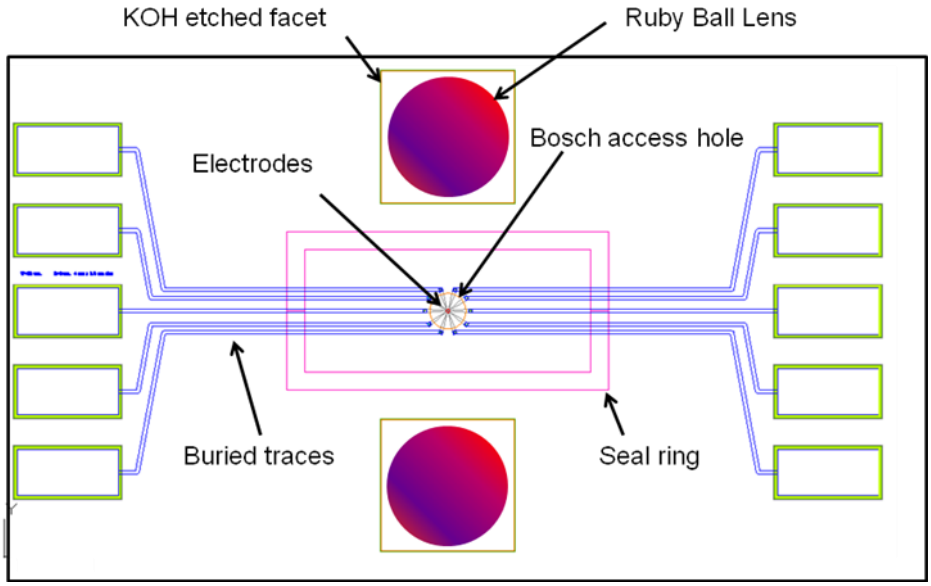

Figure A9. Bottom Prototype 2 TEM chip design for the Ball Lens Alignment.

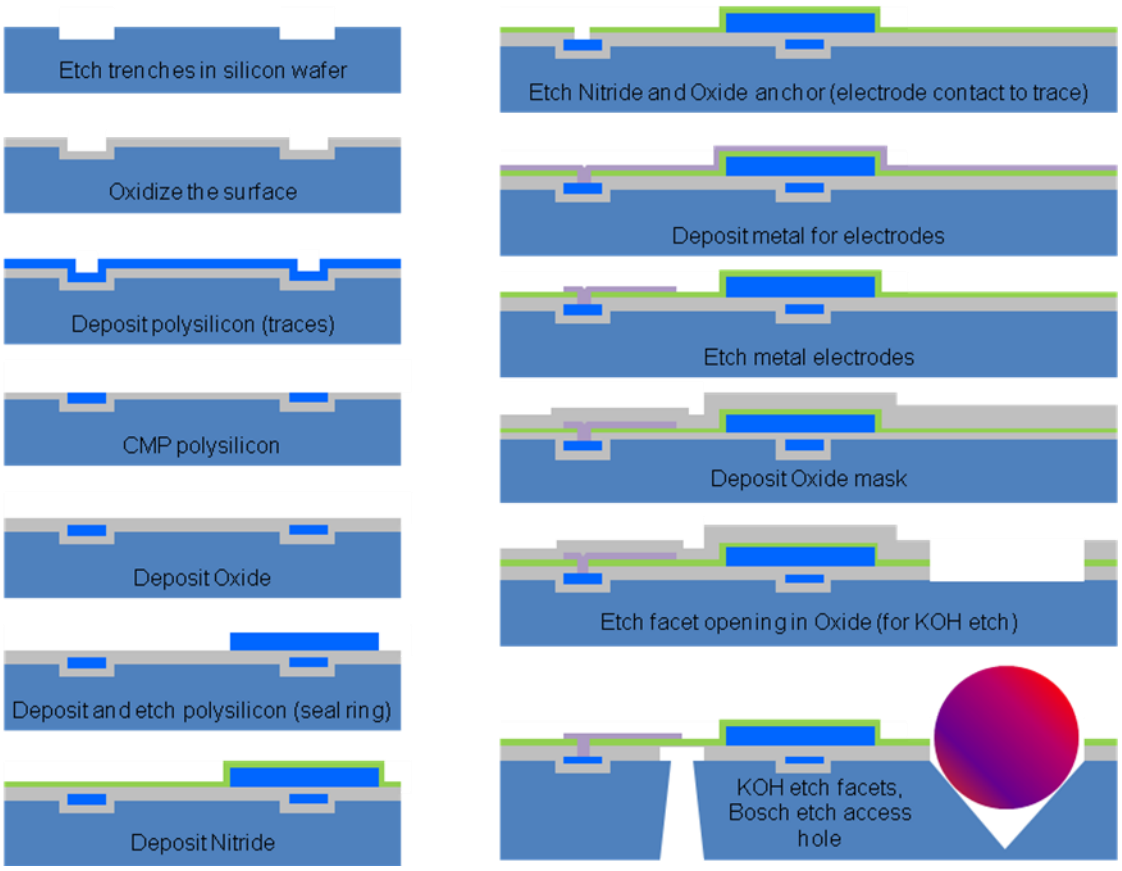

Figure A10. Process details for the Bottom Prototype 2 Ball Lens alignment chip.

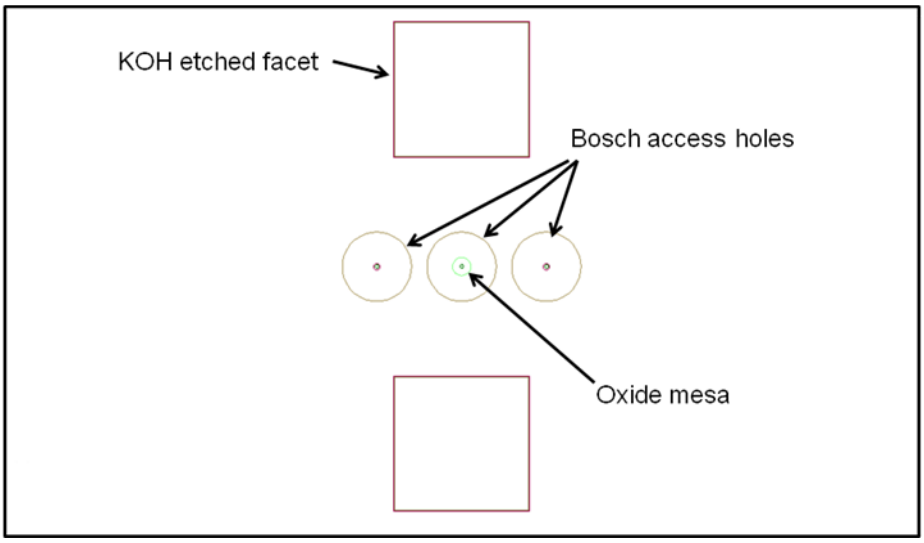

Figure A11. Top Prototype 2 *in-situ* TEM chip design for the Ball Lens alignment.

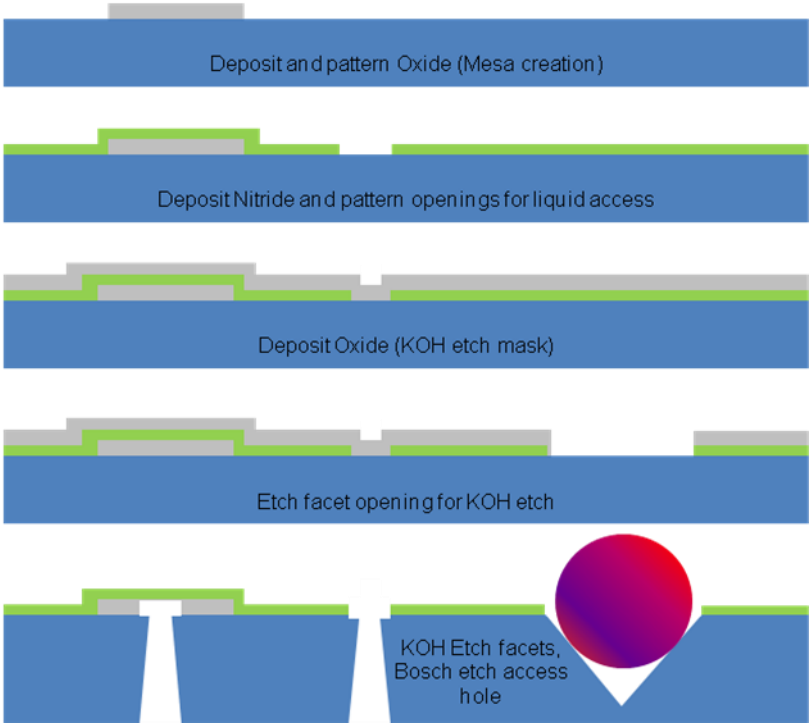

Figure A12. Process details for the Top Prototype 2 Ball Lens alignment chip.

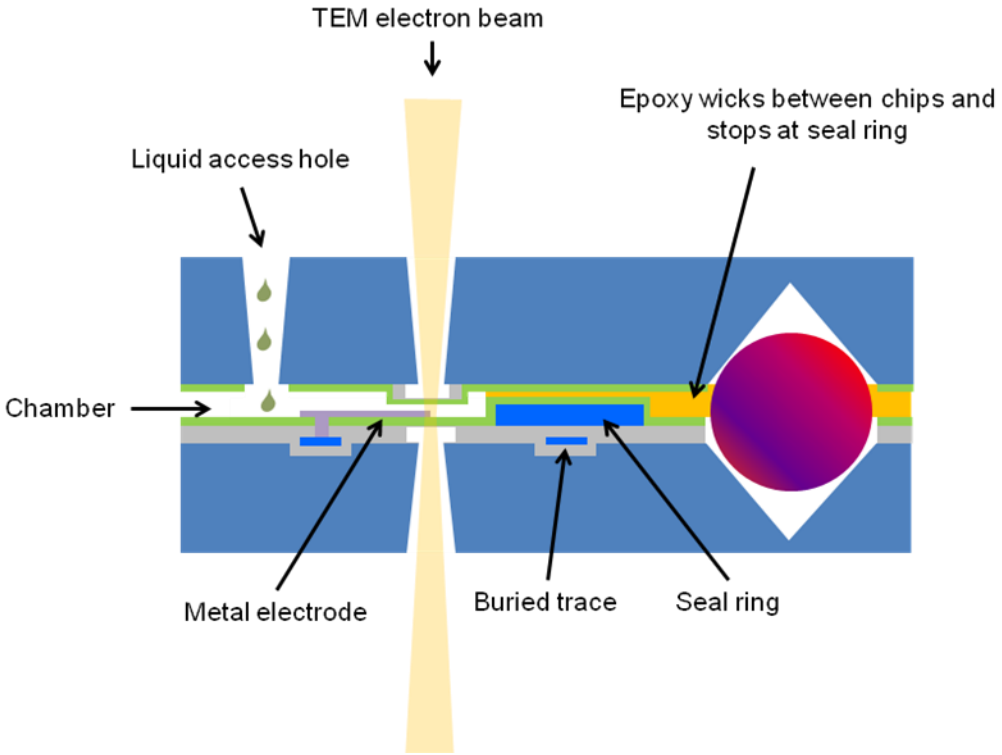

Figure A13. Assembly of the Prototype 2 Ball Lens alignment chip.

DISTRIBUTION

1	MS0359	D. Chavez, LDRD Office	1911
1	MS1304	John P. Sullivan	01132
1	MS1315	Sean J. Hearne	01132
1	MS0899	RIM-Reports Management	9532 (electronic copy)


Sandia National Laboratories